Supplement of Earth Syst. Sci. Data, 18, 3559–3585, 2026
https://doi.org/10.5194/essd-18-3559-2026-supplement

Open Access Earth System Science Data

Supplement of

A dataset of vertical profiles of O_3 and HONO from the hyperspectral vertical remote sensing network in China (2021–2024)

Tiliang Zou et al.

Correspondence to: Chengzhi Xing (xingcz@aiofm.ac.cn) and Cheng Liu (chliu81@ustc.edu.cn)

Table S1. Locations of all sites and their nearest CNEMCs stations.

MAX-DOAS stations				The nearest CNEMCs			Distance
No.	Station(code)	Longitude(°E)	Latitude(°N)	Station(code)	Longitude(°E)	Latitude(°N)	(km)
1	CAMS1	116.32	39.94	1006A	116.34	39.93	2.01
2	CAMS2	116.32	39.94	1006A	116.34	39.93	2.01
3	UCAS	116.67	40.4	1009A	116.63	40.33	8.83
4	WD	115.15	38.17	3573A	114.85	38.03	30.34
5	SJZ_LC	114.61	37.91	3572A	114.64	37.90	3.01
6	SXU	112.58	37.63	1085A	112.56	37.74	12.31
7	TS	117.1	36.25	1657A	117.09	36.20	5.47
8	NUIST	118.71	32.2	1157A	118.64	32.09	13.53
9	LA	119.75	30.3	3558A	119.72	30.24	7.67
10	HNU	116.8	33.98	2282A	116.80	33.98	0.56
11	AHU	117.18	31.77	1270A	117.20	31.78	2.23
12	CF	117.18	32.21	1275A	117.27	31.94	30.71
13	GIG	113.35	23.15	2846A	113.32	23.13	3.47
14	SUST	113.99	22.59	3306A	114.03	22.62	4.97
15	CDAES	104.04	30.65	1437A	104.04	30.66	0.69
16	CQ	106.5	29.6	3133A	106.55	29.57	5.94
17	GZ_ZL	113.34	23.36	3299A	113.35	23.37	1.26
18	GZ_NS	113.61	22.77	3304A	113.53	22.79	8.07
19	GZ_TM	113.29	23.55	3443A	113.29	23.55	0.49
20	GZ_GY	113.26	23.13	1352A	113.26	23.13	0.35
21	GZ_DXC	113.39	23.04	3302A	113.39	23.05	1.02
22	LY	112.45	34.67	3636A	112.44	34.68	1.36

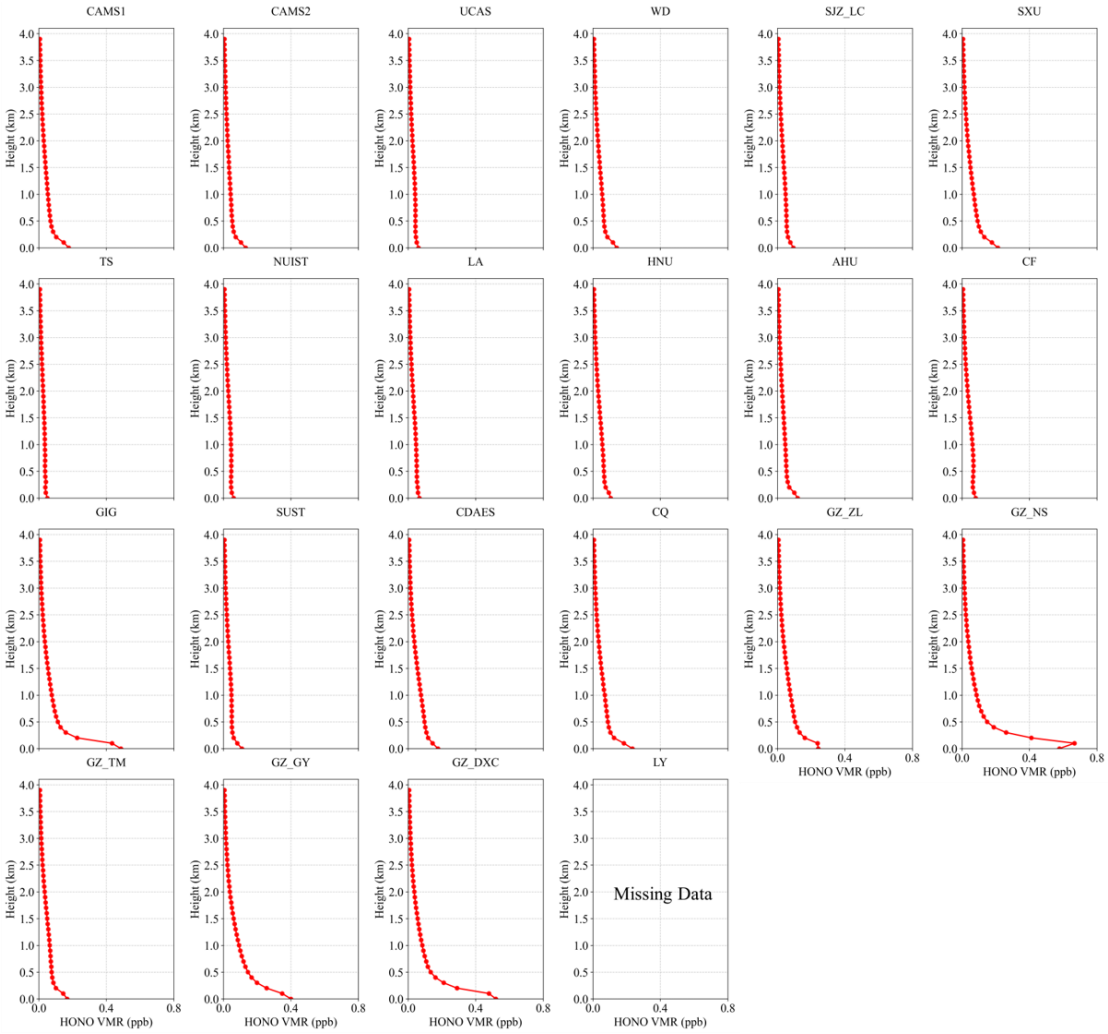

Figure S1. Seasonal-mean vertical profiles of HONO in spring (2021–2024).

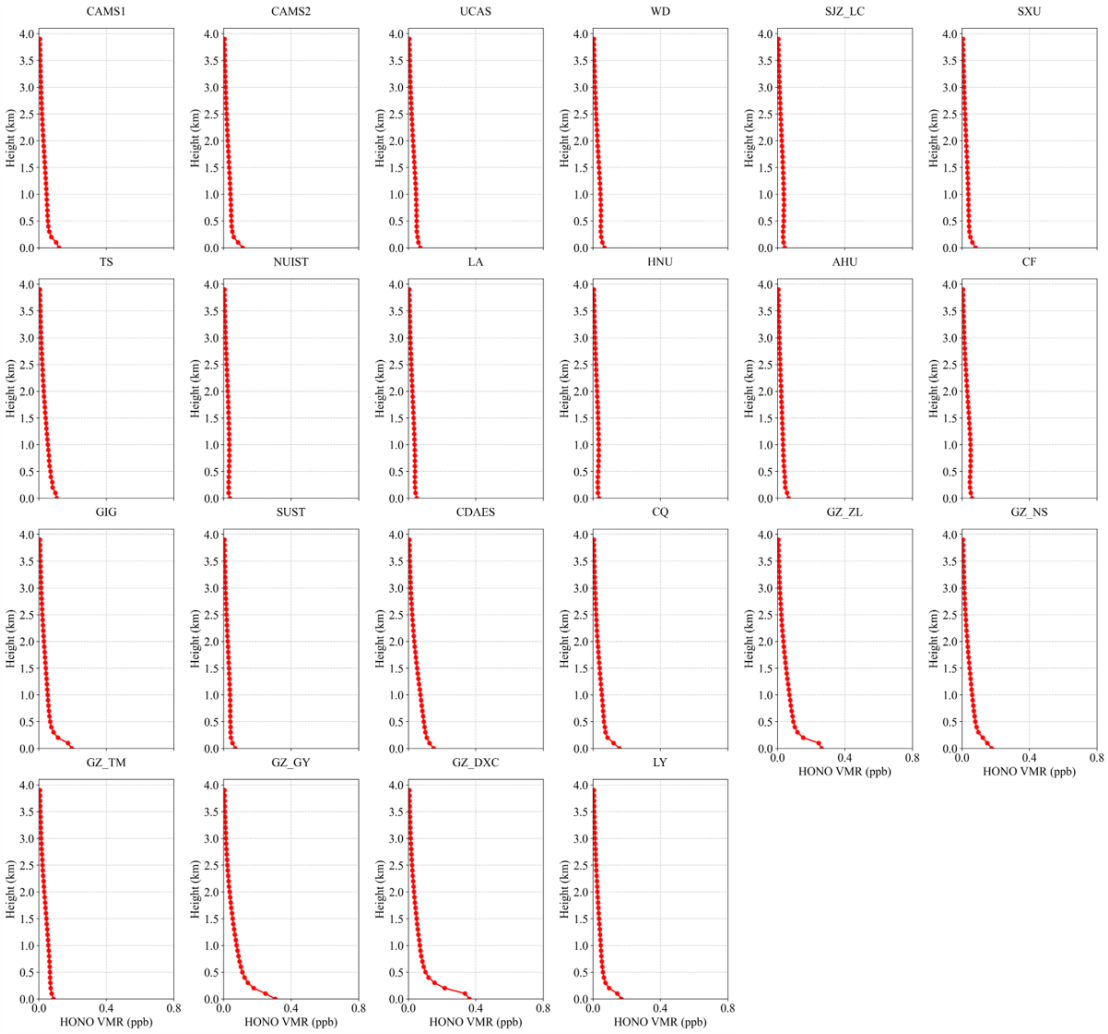

Figure S2. Seasonal-mean vertical profiles of HONO in summer (2021–2024).

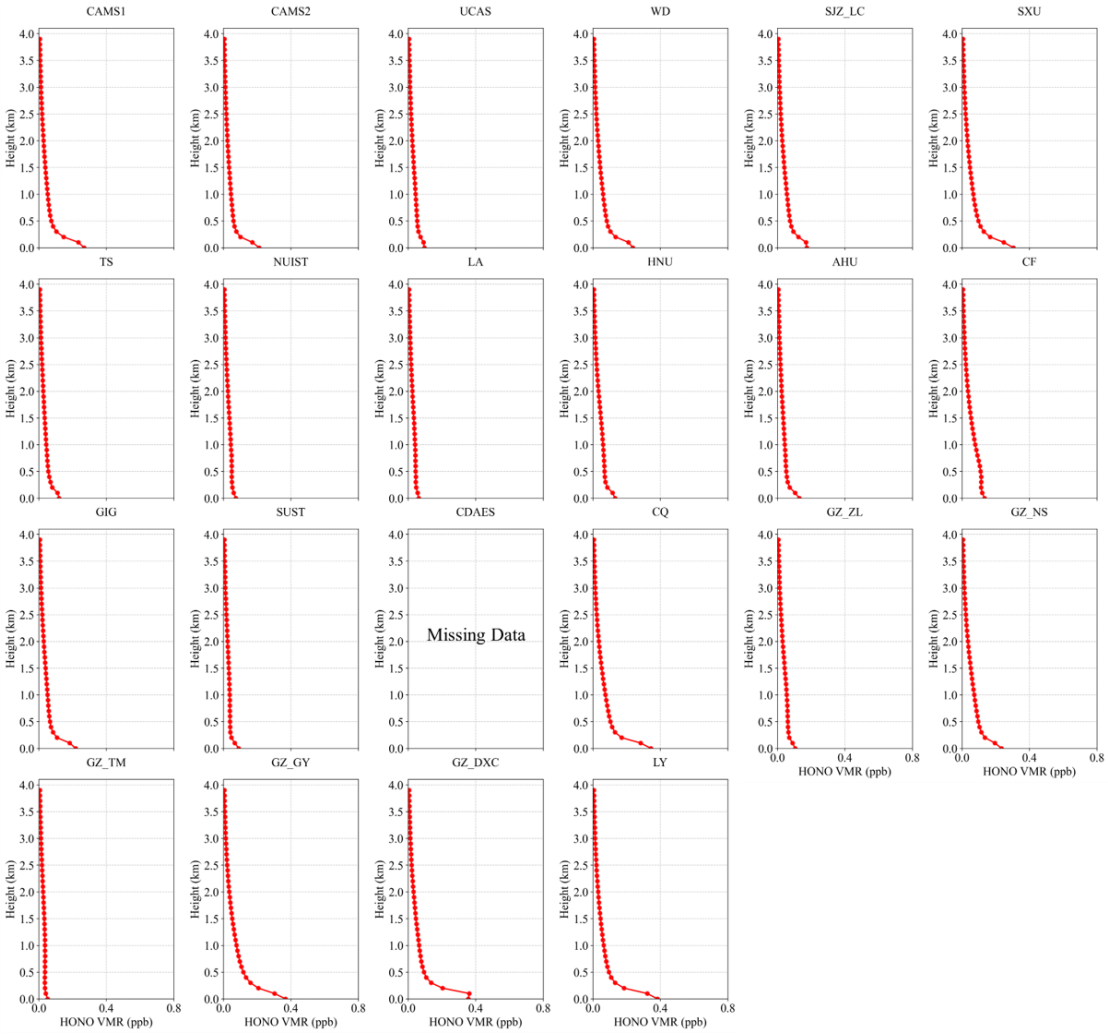

Figure S3. Seasonal-mean vertical profiles of HONO in autumn (2021–2024).

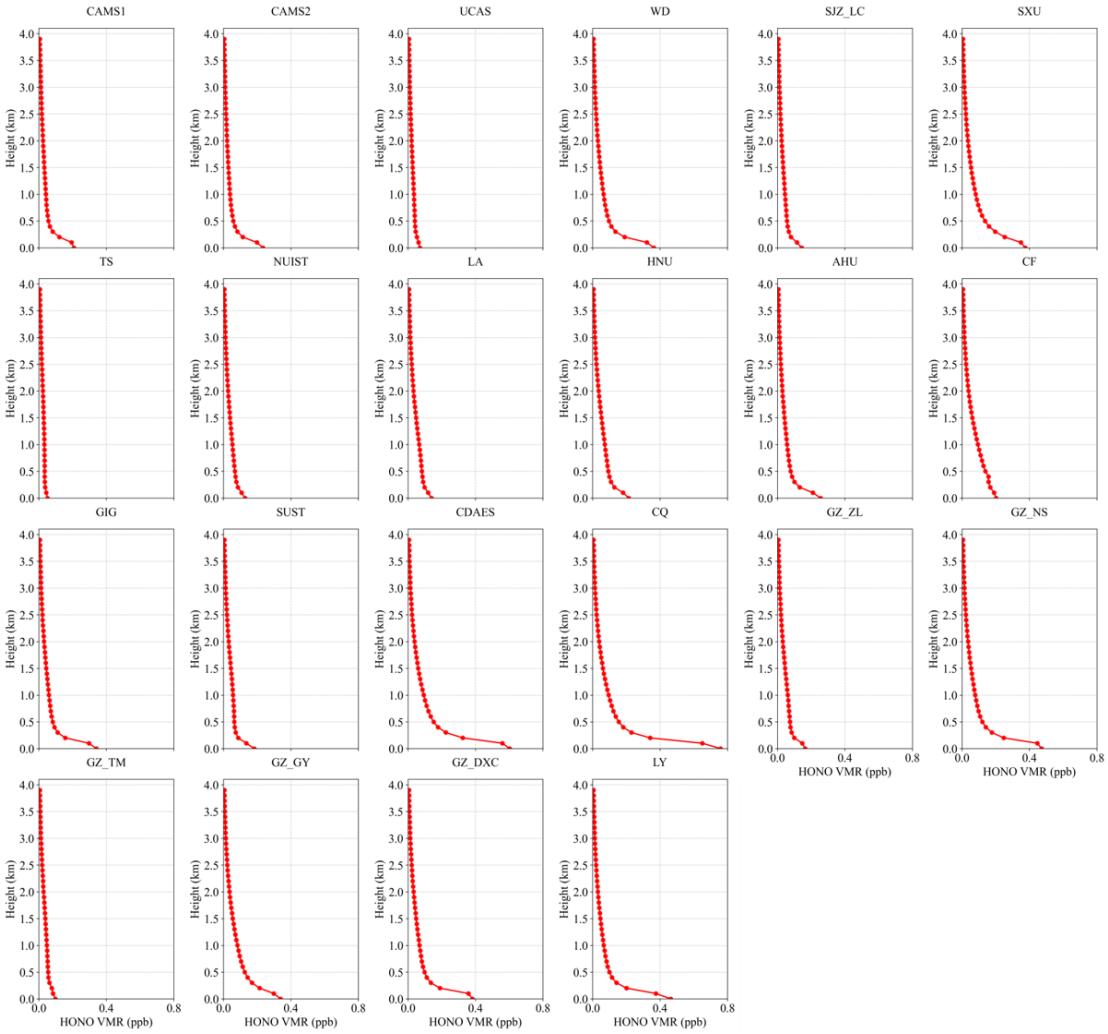

Figure S4. Seasonal-mean vertical profiles of HONO in winter (2021–2024).

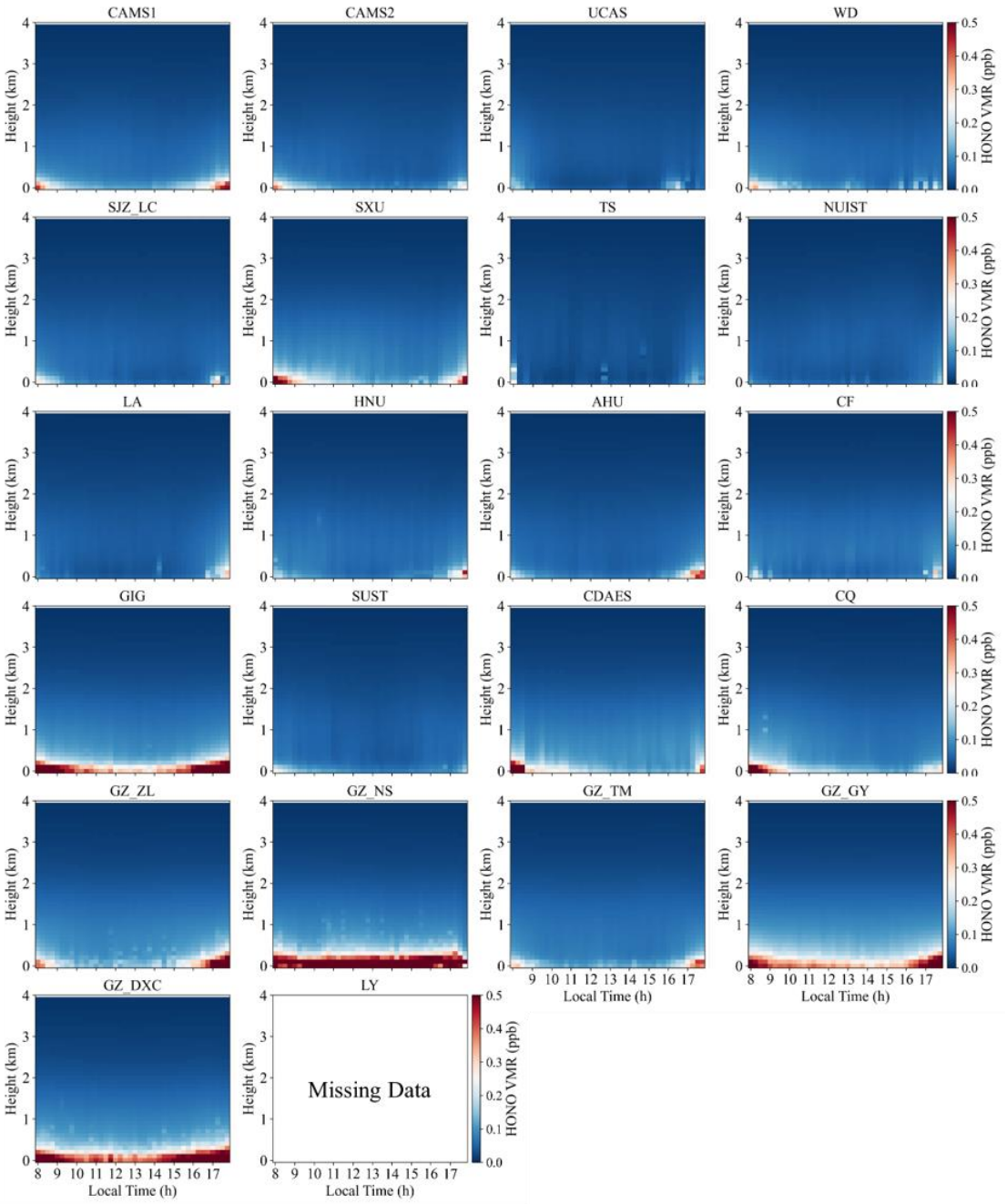

Figure S5. Mean diurnal evolution of the springtime HONO vertical profiles (2021–2024).

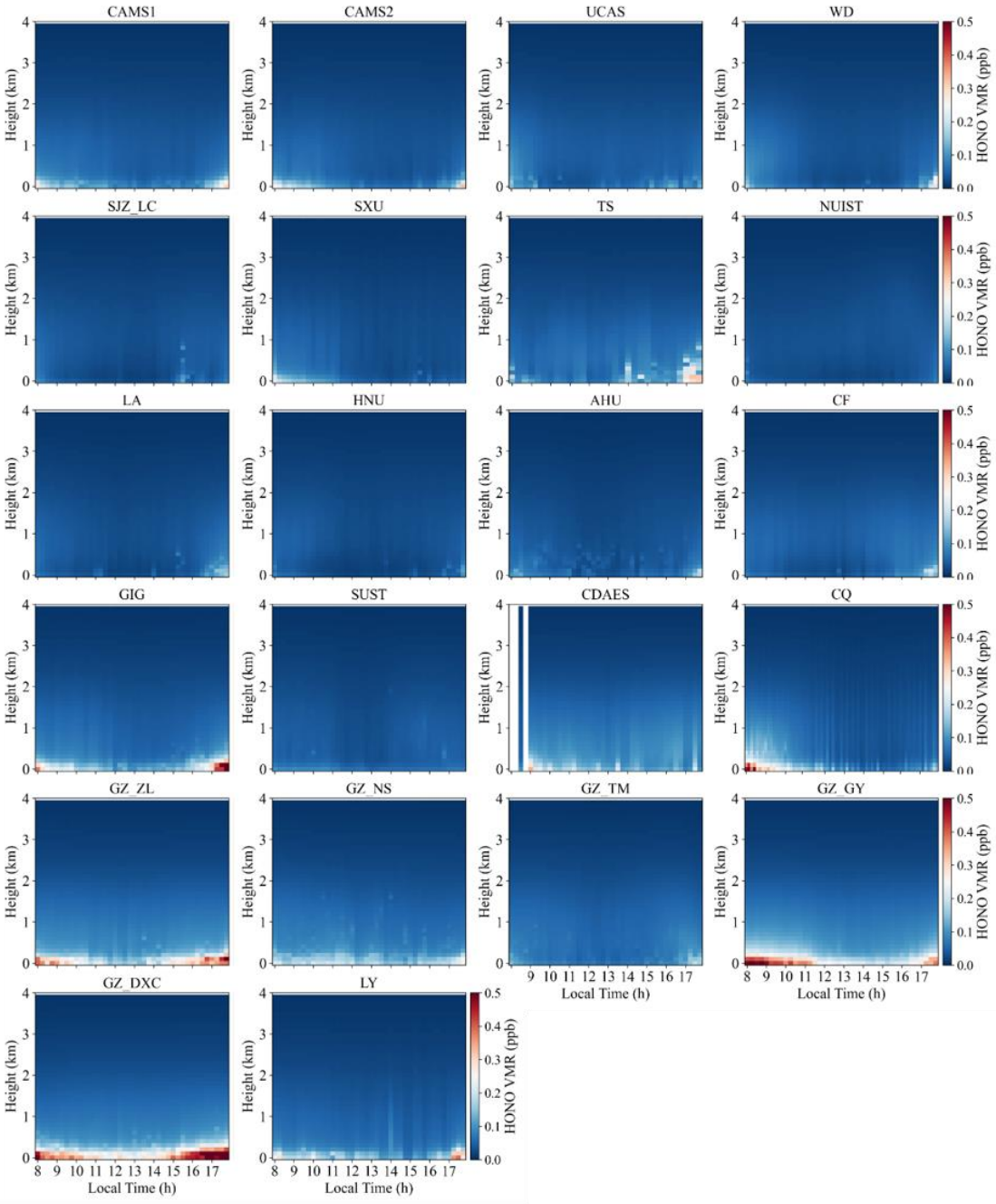

Figure S6. Mean diurnal evolution of the summertime HONO vertical profiles (2021–2024).

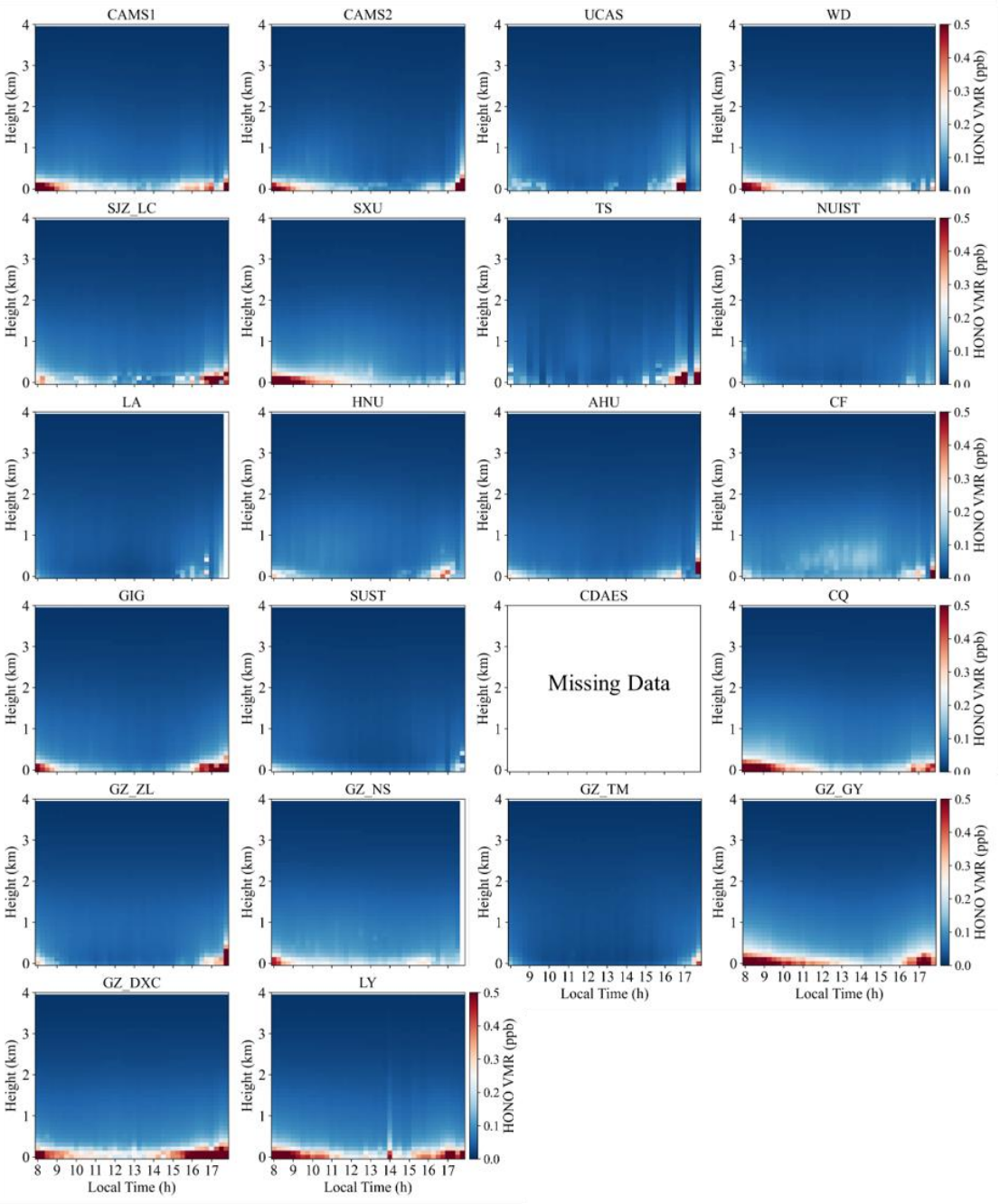

Figure S7. Mean diurnal evolution of the autumnal HONO vertical profiles (2021–2024).

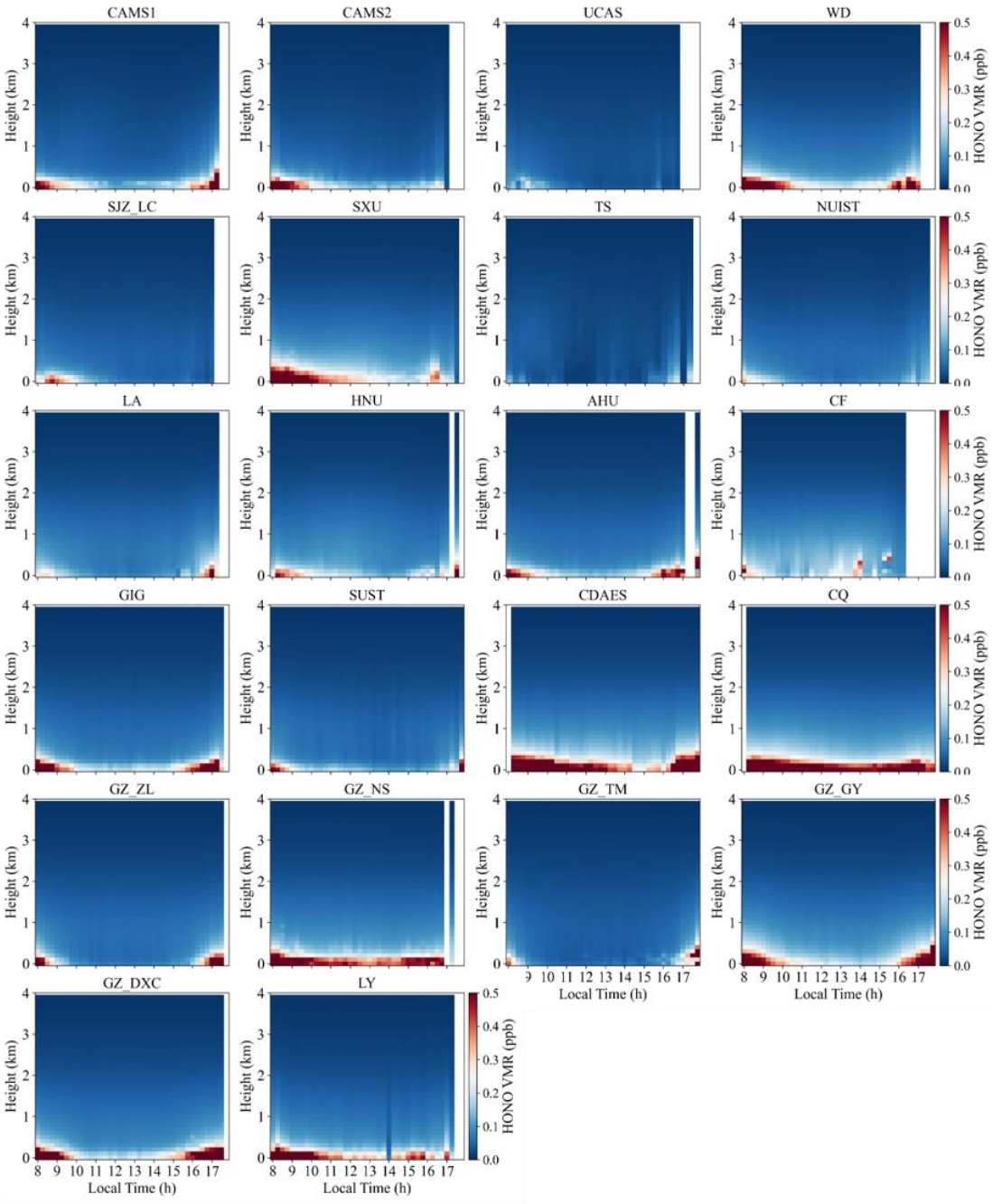

Figure S8. Mean diurnal evolution of the wintertime HONO vertical profiles (2021–2024).

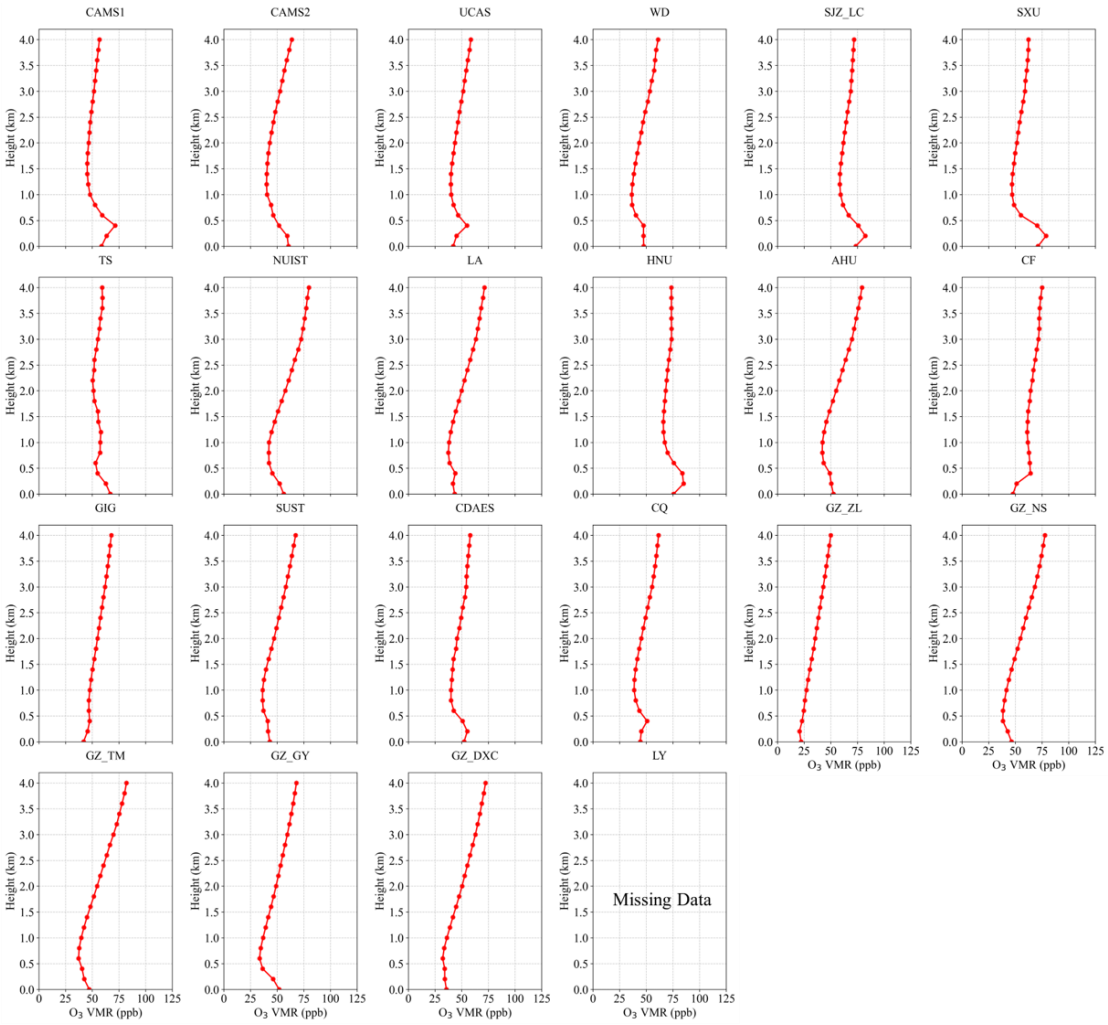

Figure S9. Seasonal-mean vertical profiles of O_3 in spring (2021–2024).

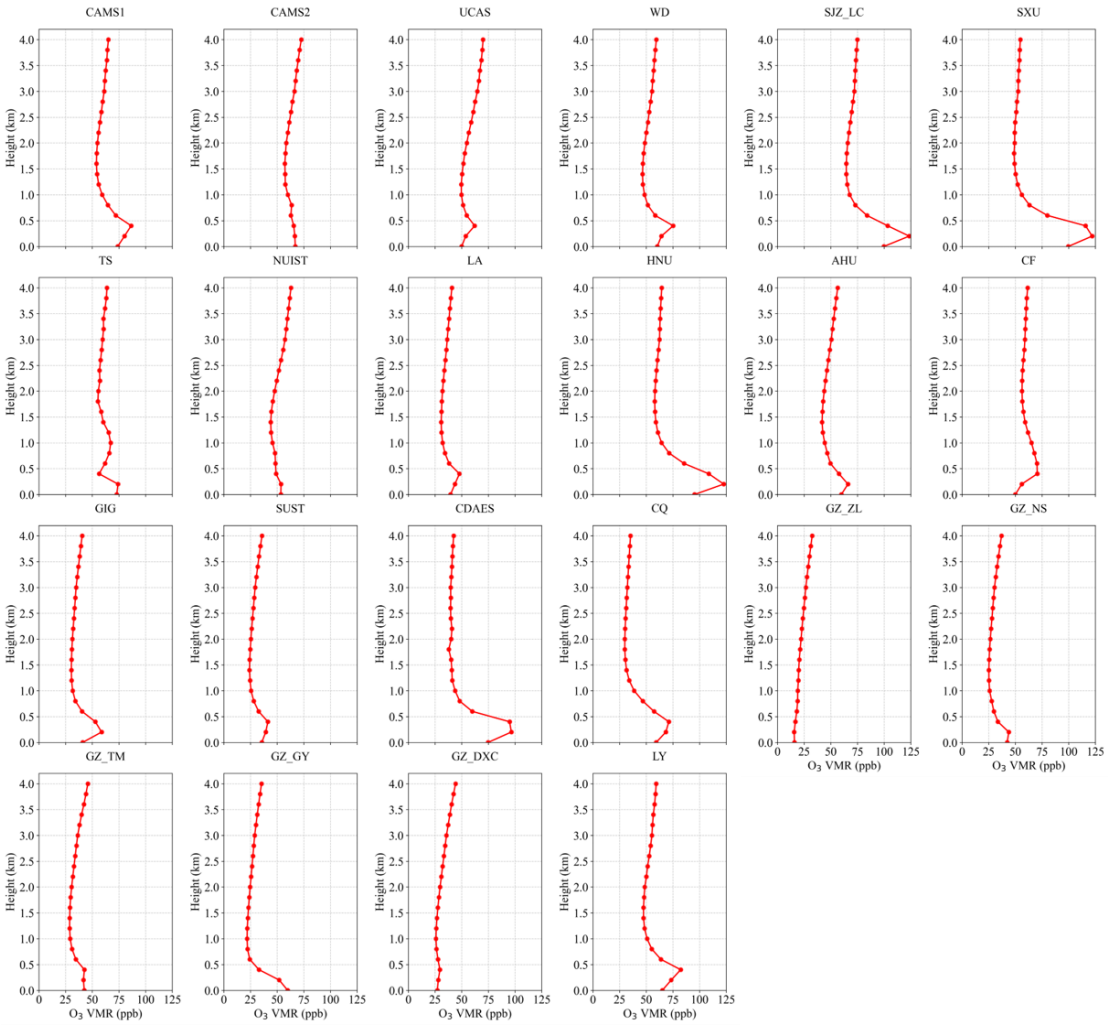

Figure S10. Seasonal-mean vertical profiles of O_3 in summer (2021–2024).

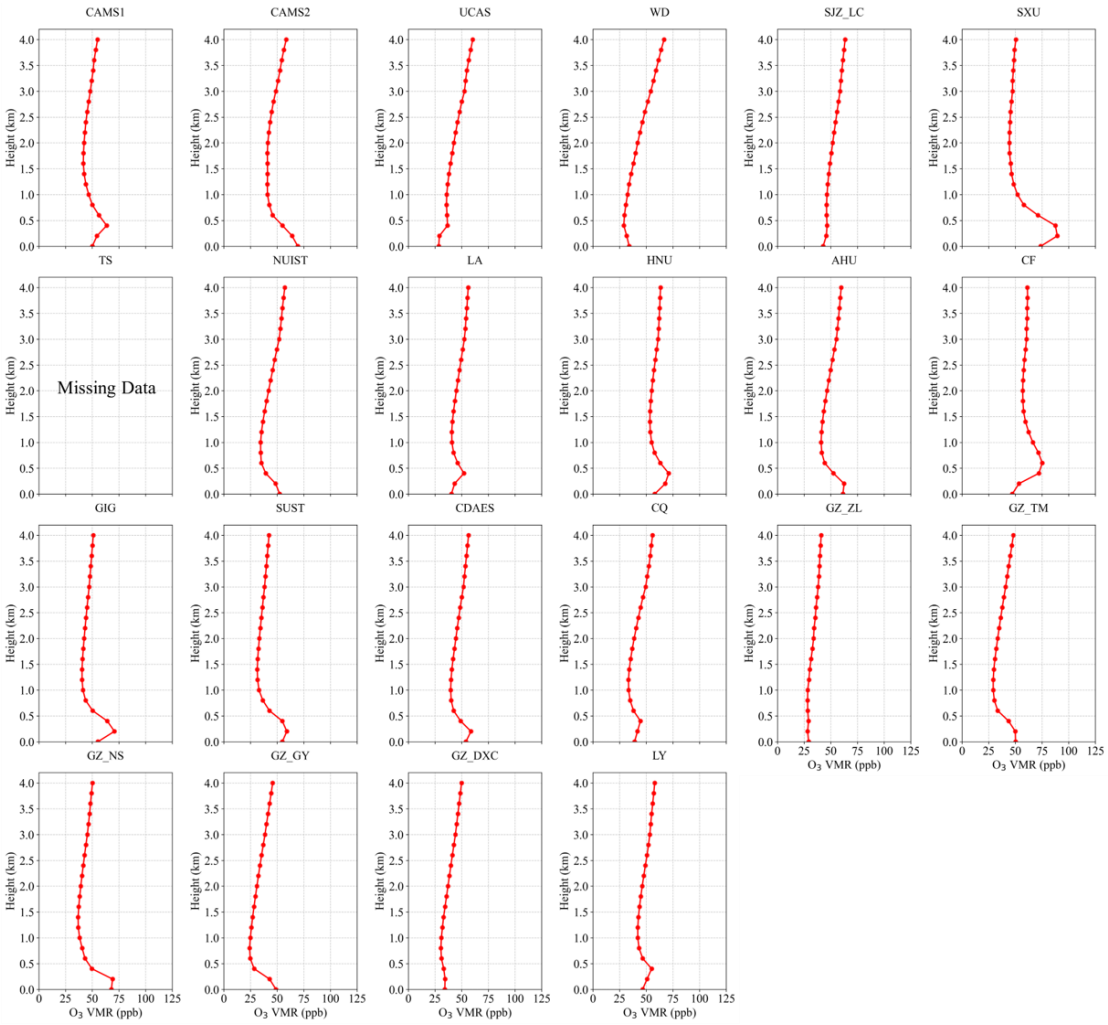

Figure S11. Seasonal-mean vertical profiles of O_3 in autumn (2021–2024).

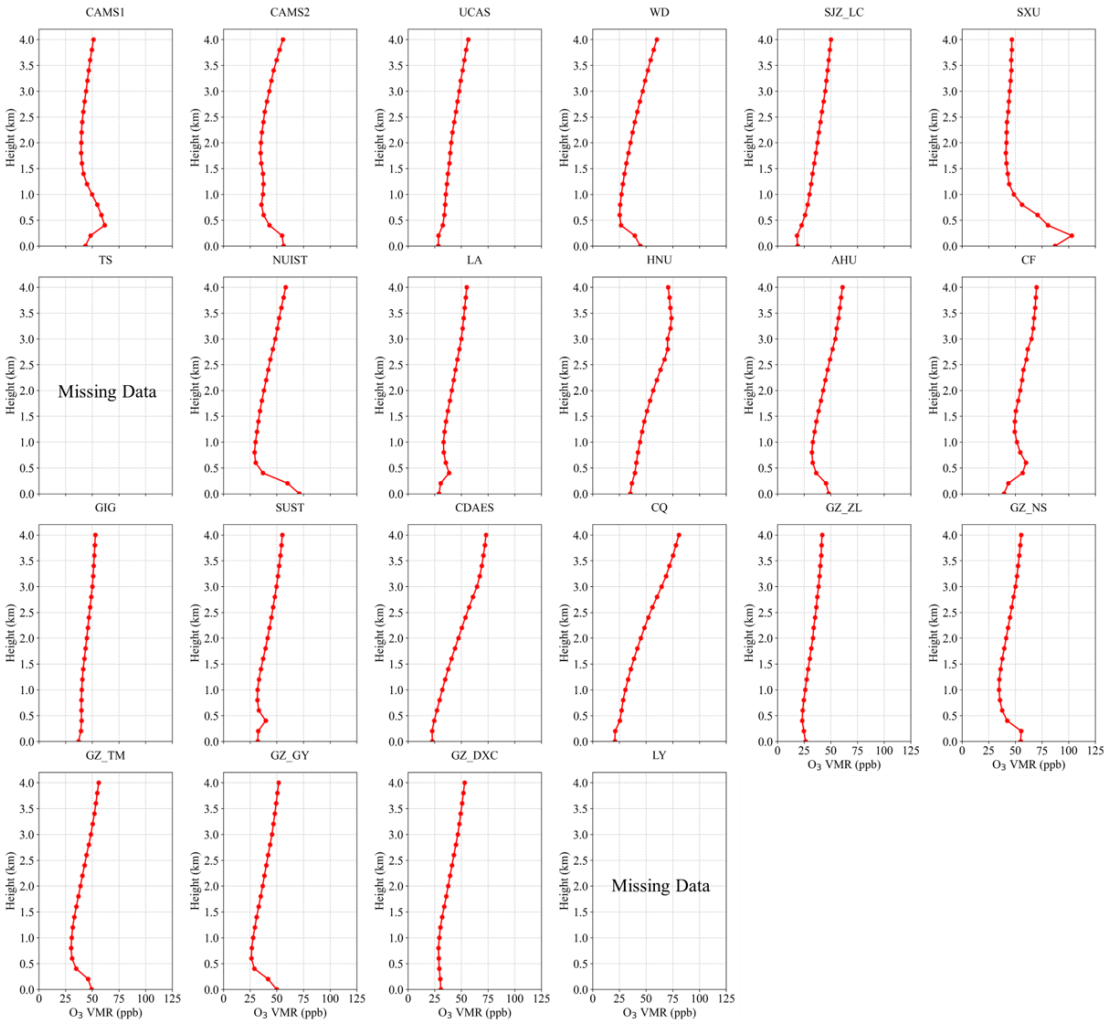

Figure S12. Seasonal-mean vertical profiles of O_3 in winter (2021–2024).

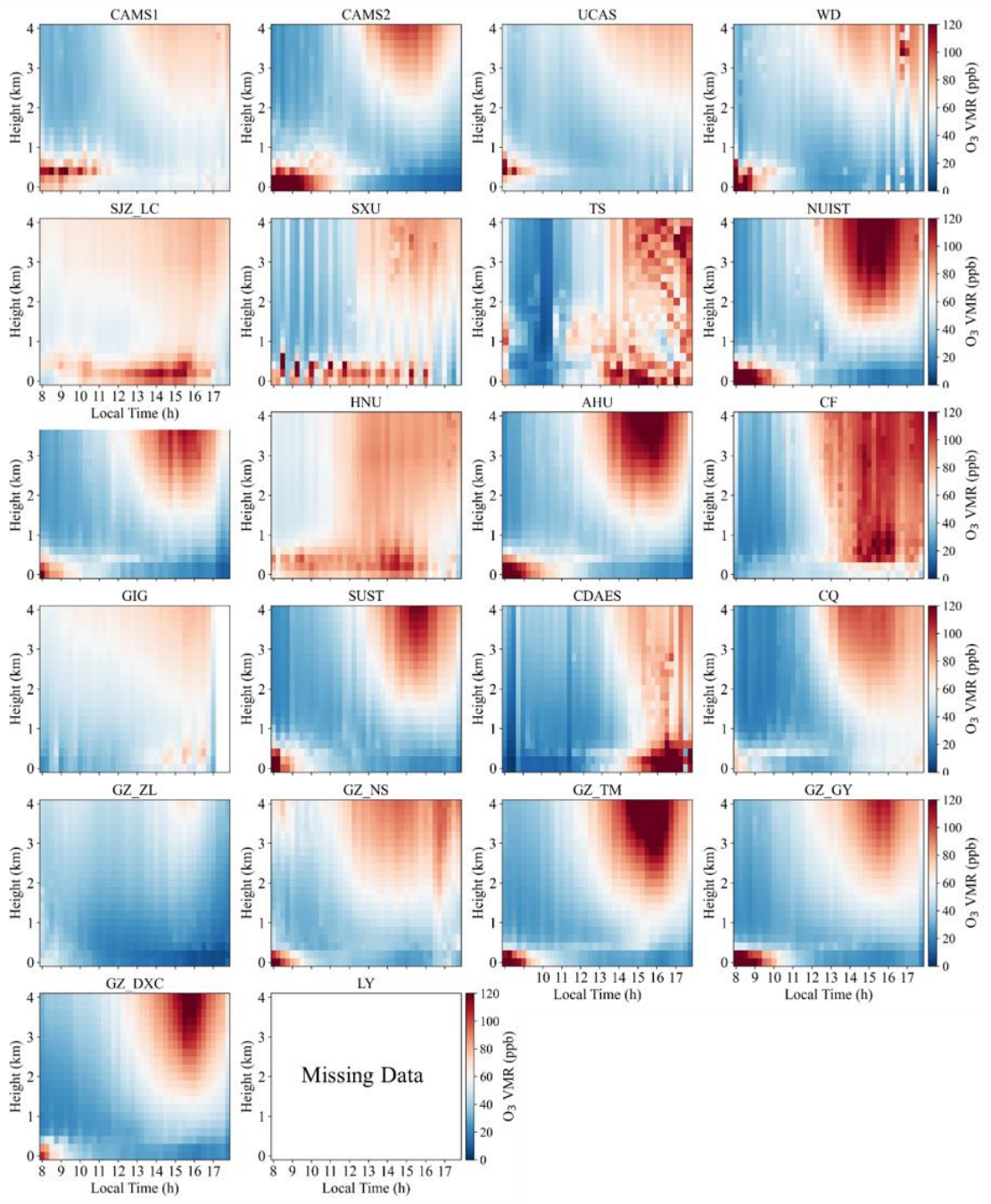

Figure S13. Mean diurnal evolution of the springtime O_3 vertical profiles (2021–2024).

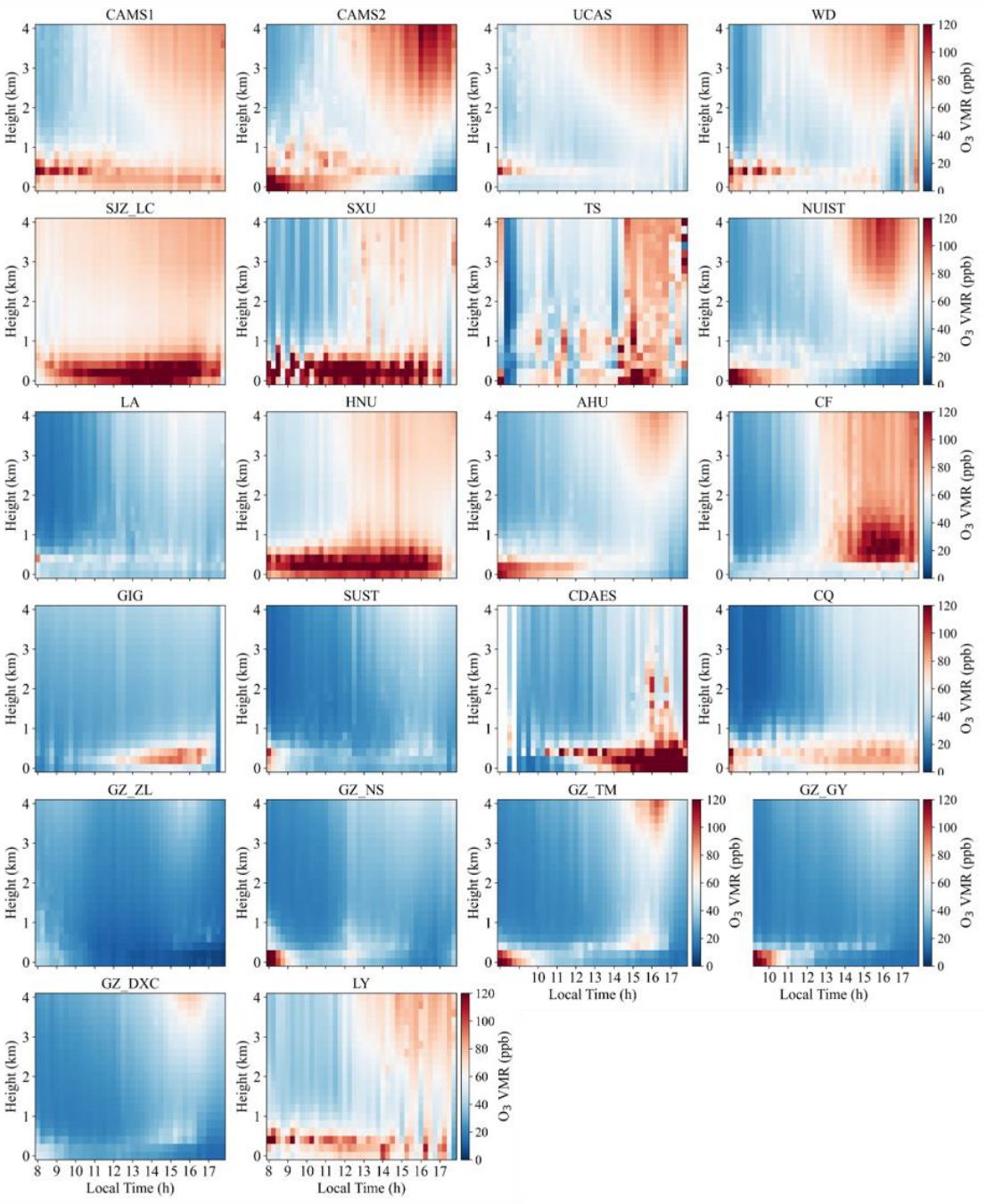

Figure S14. Mean diurnal evolution of the summertime O_3 vertical profiles (2021–2024).

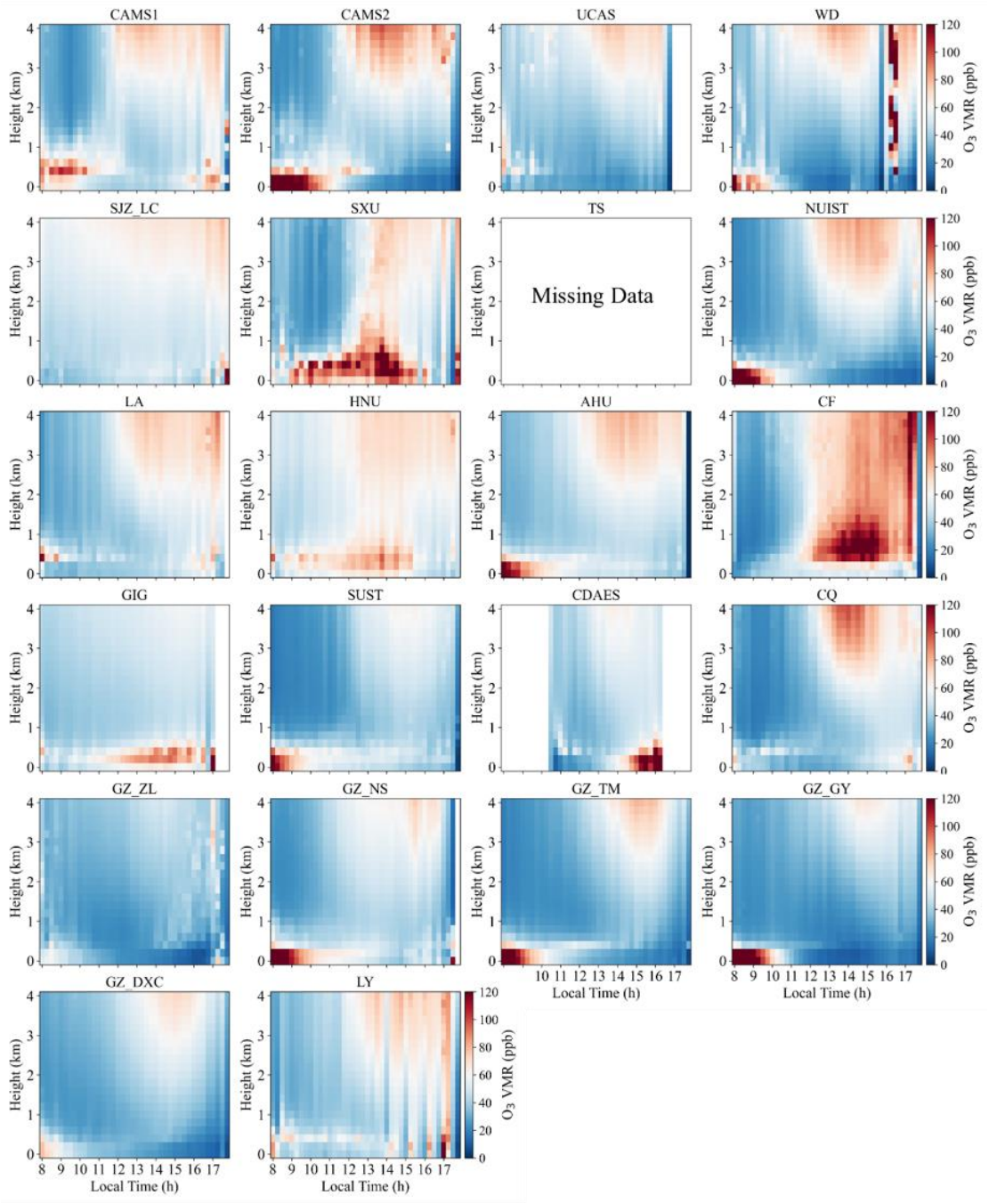

Figure S15. Mean diurnal evolution of the autumnal O_3 vertical profiles (2021–2024).

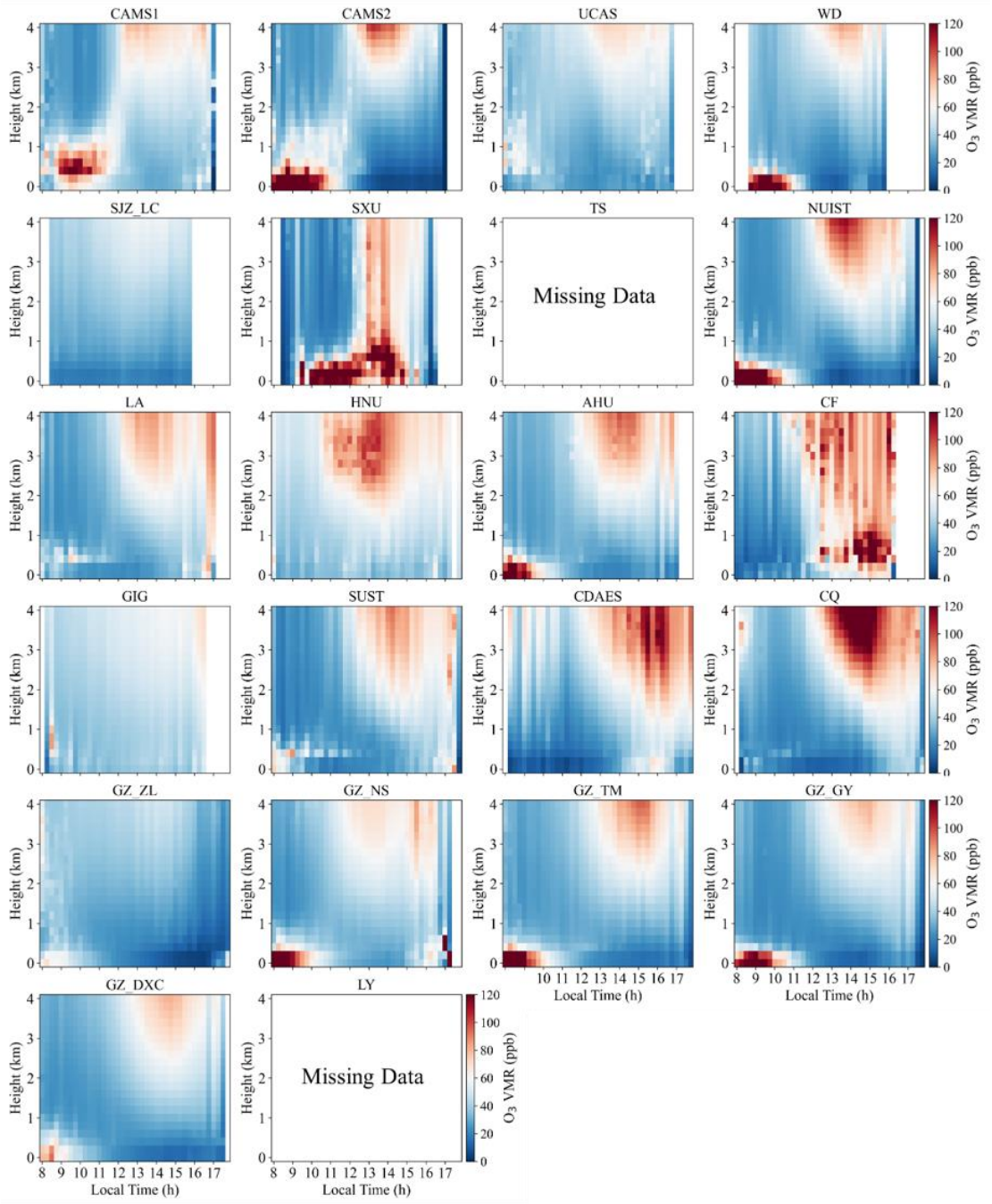

Figure S16. Mean diurnal evolution of the wintertime O_3 vertical profiles (2021–2024).

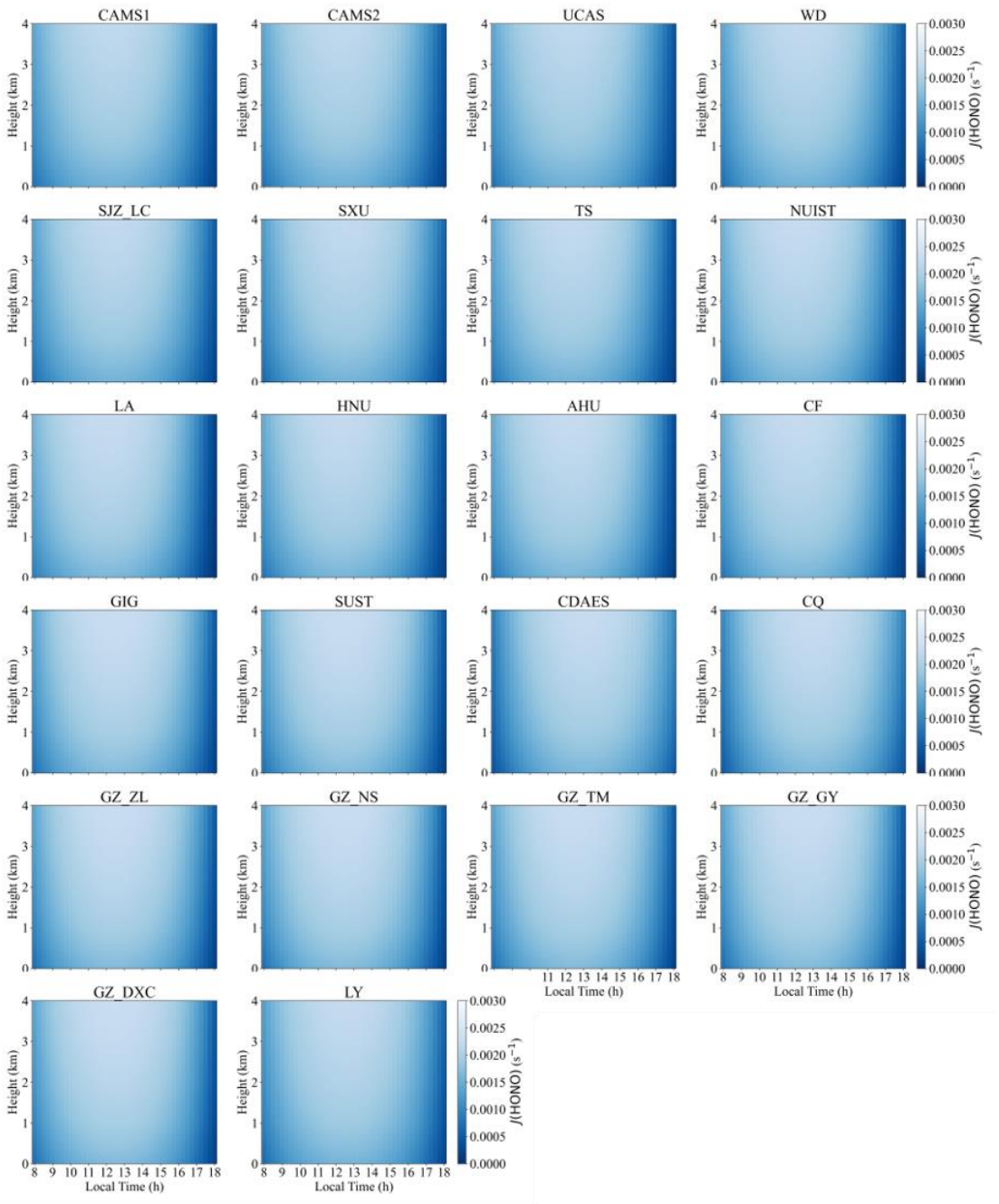

Figure S17. Spring-mean diurnal vertical profiles of the HONO photolysis frequency, J(HONO).

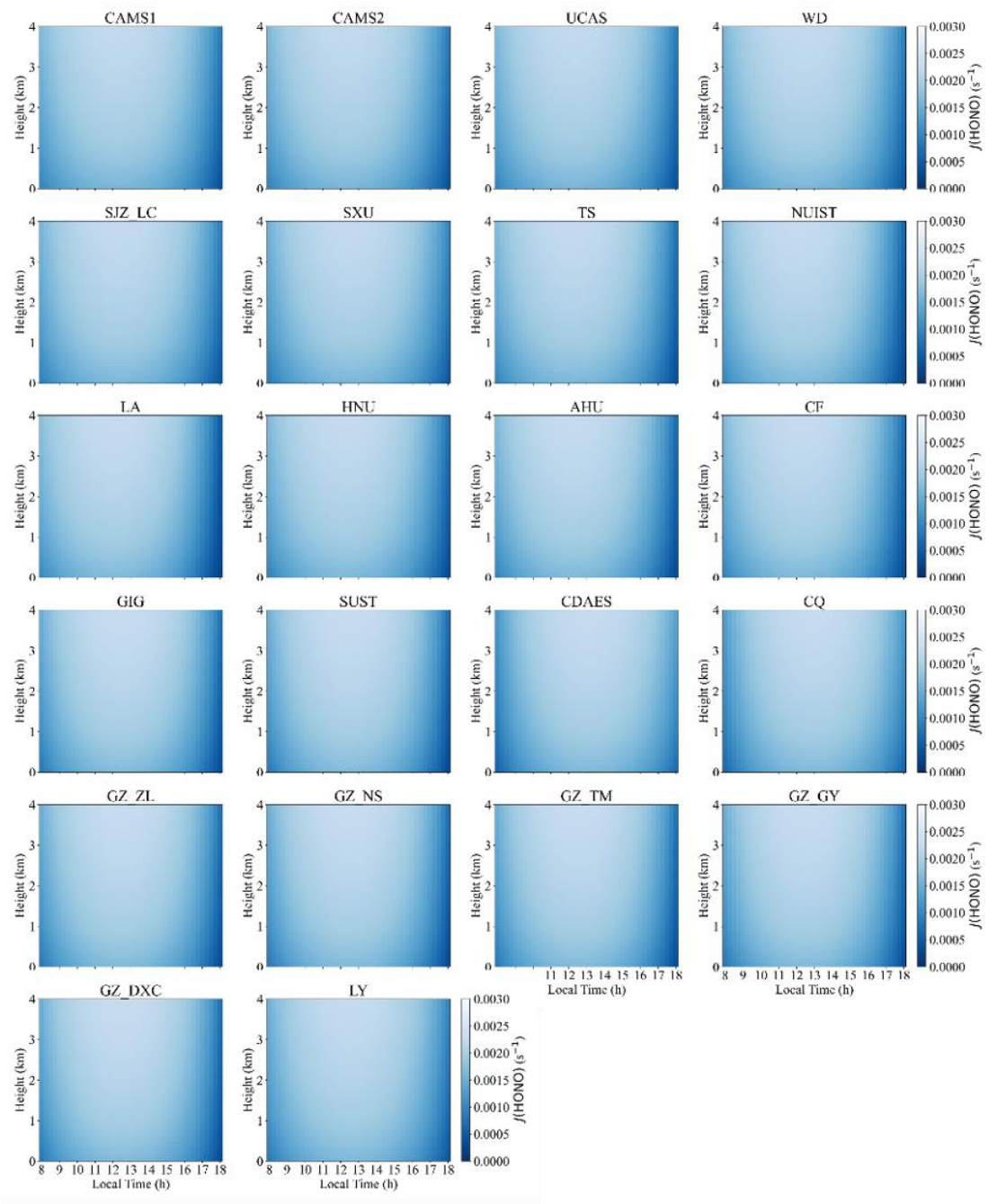

Figure S18. Summer-mean diurnal vertical profiles of the HONO photolysis frequency, J(HONO).

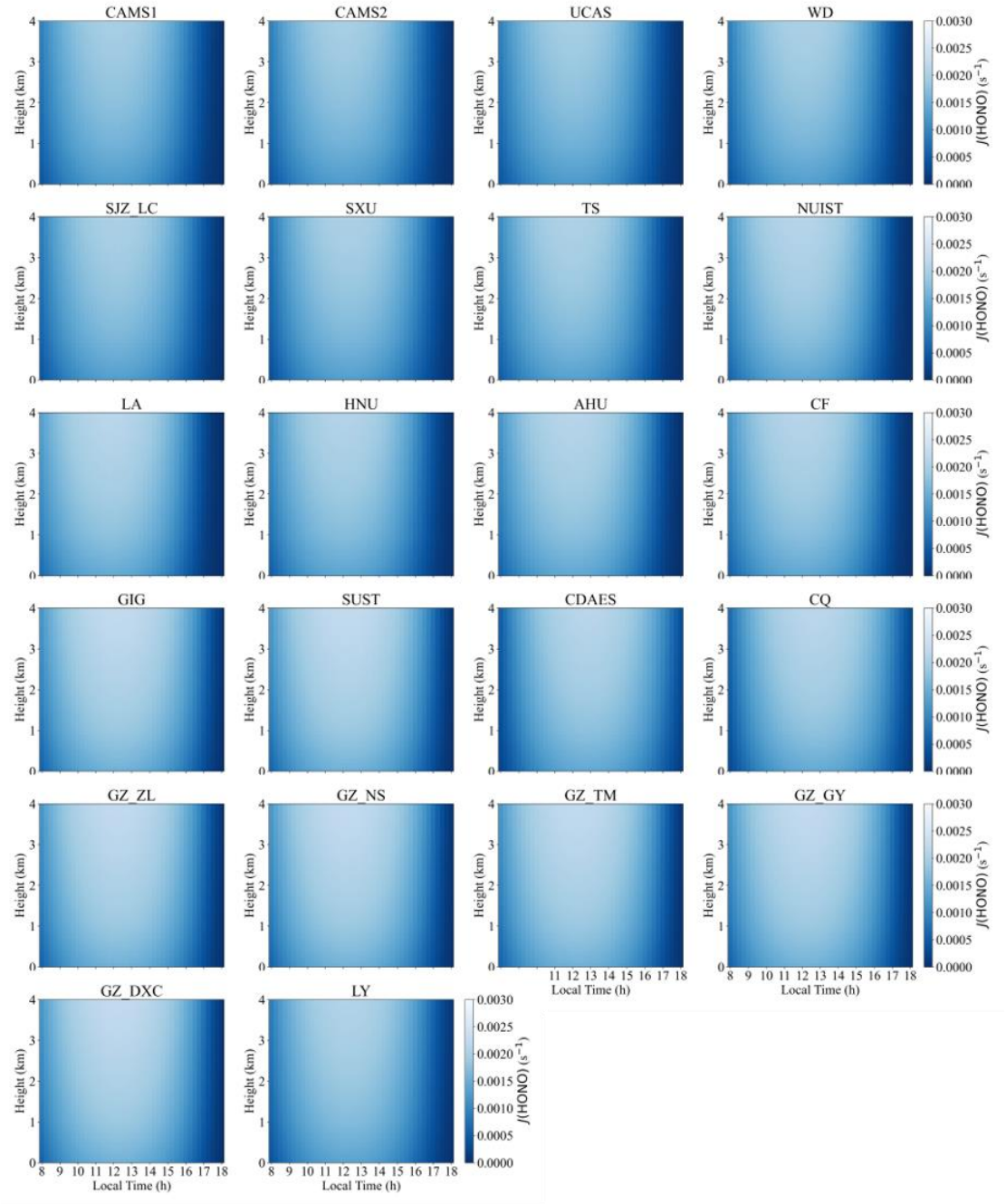

Figure S19. Autumn-mean diurnal vertical profiles of the HONO photolysis frequency, J(HONO).

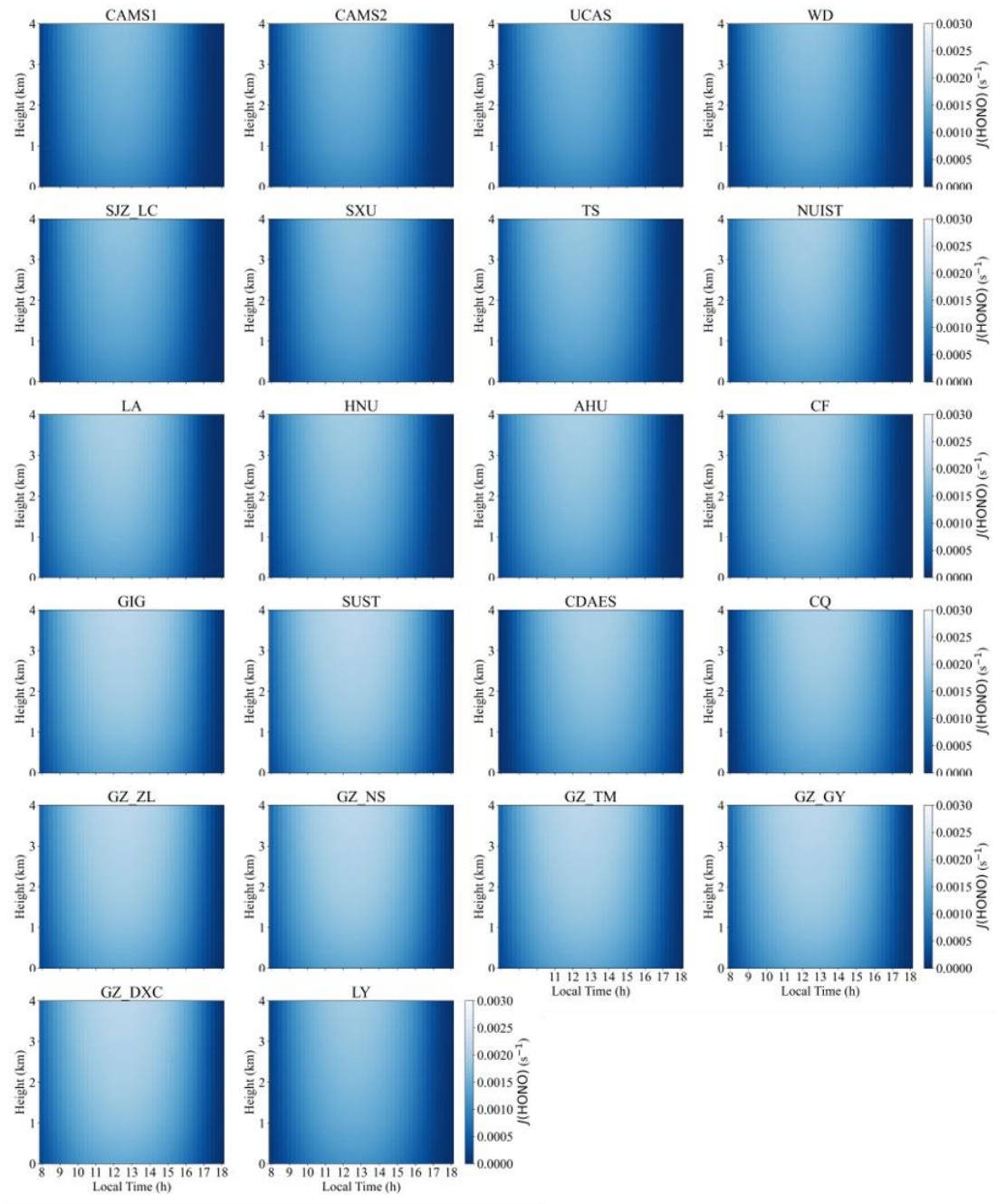

Figure S20. Winter-mean diurnal vertical profiles of the HONO photolysis frequency, J(HONO).

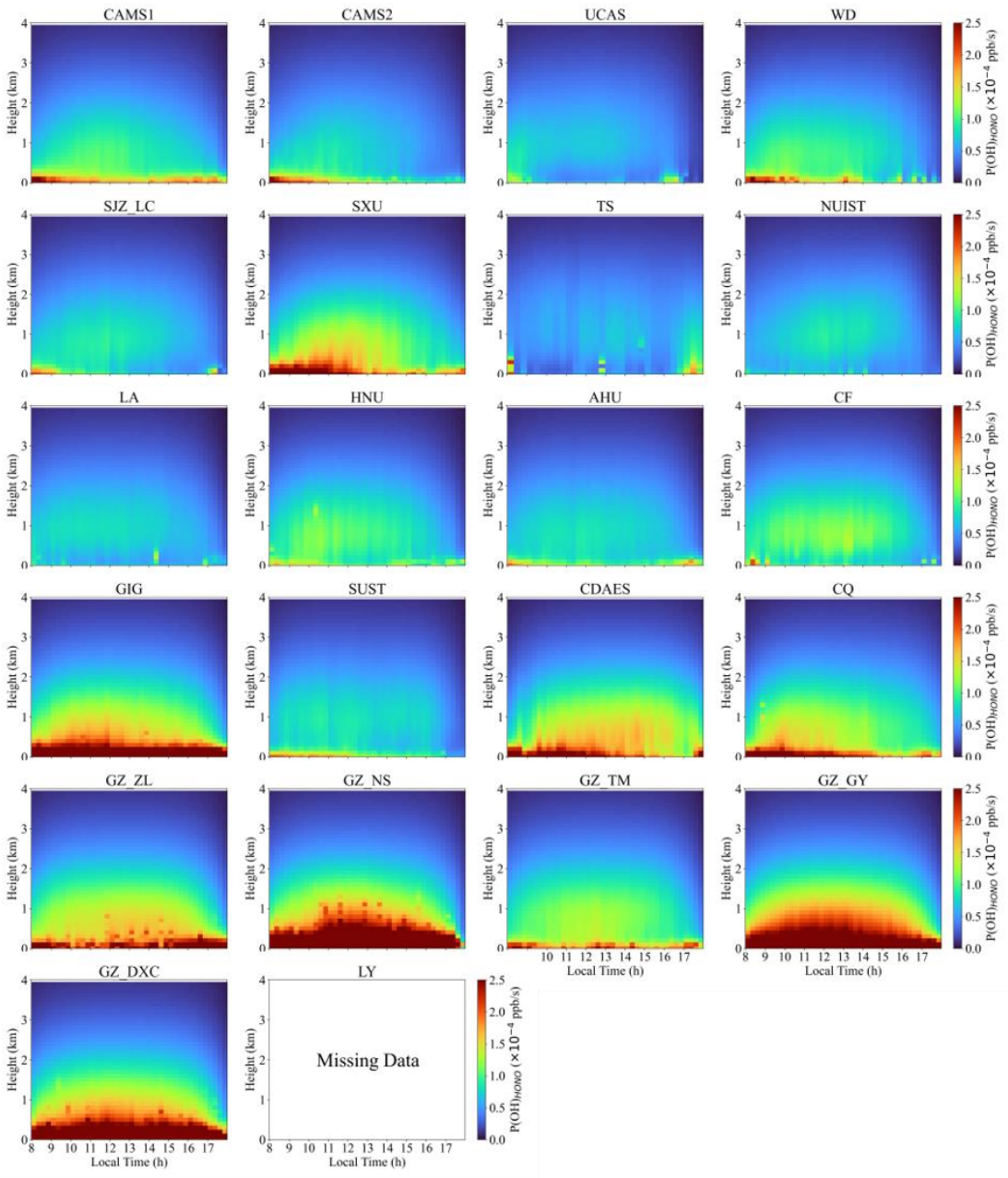

Figure S21. Spring-mean vertical profiles of OH production from HONO photolysis.

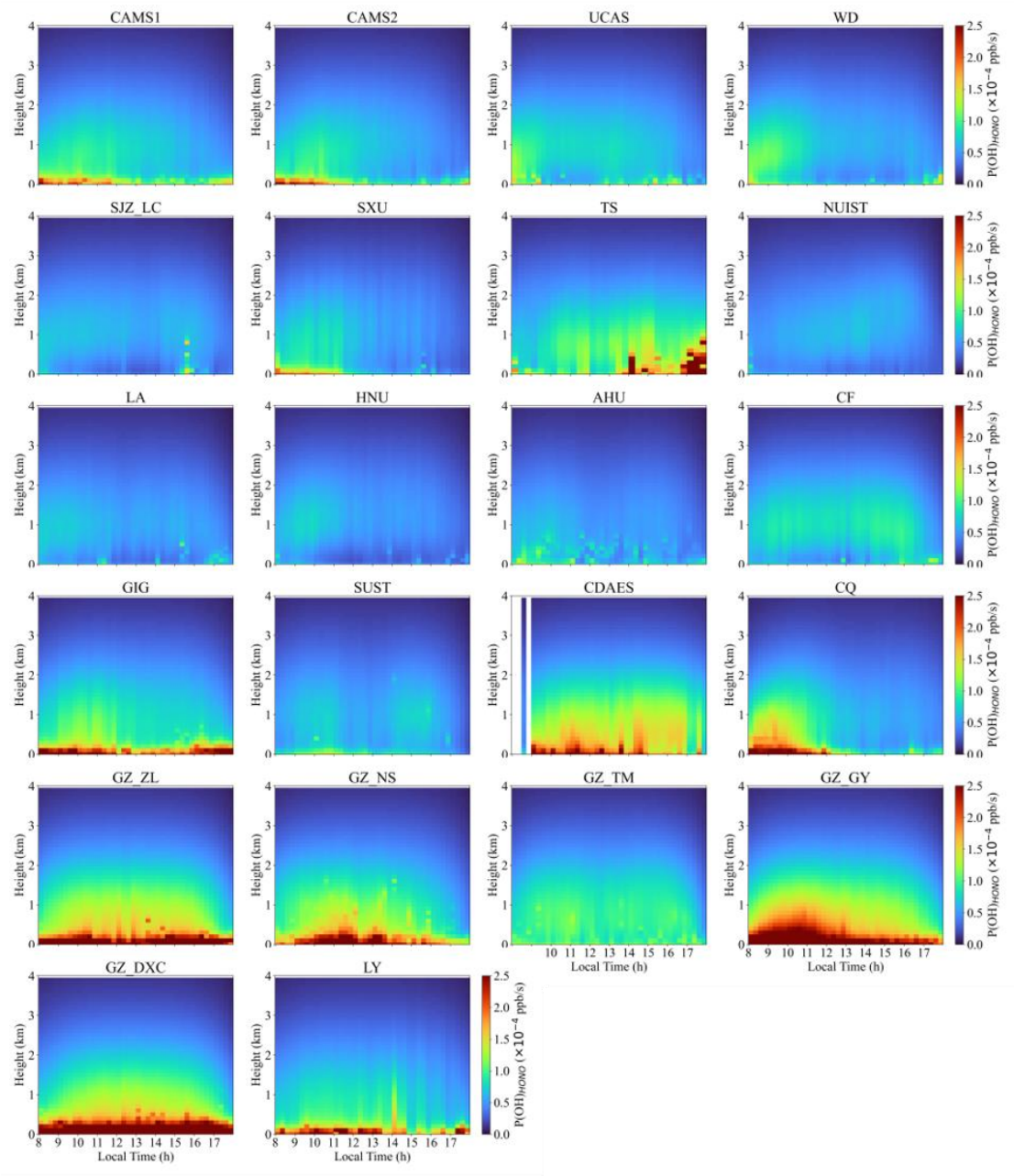

Figure S22. Summer-mean vertical profiles of OH production from HONO photolysis.

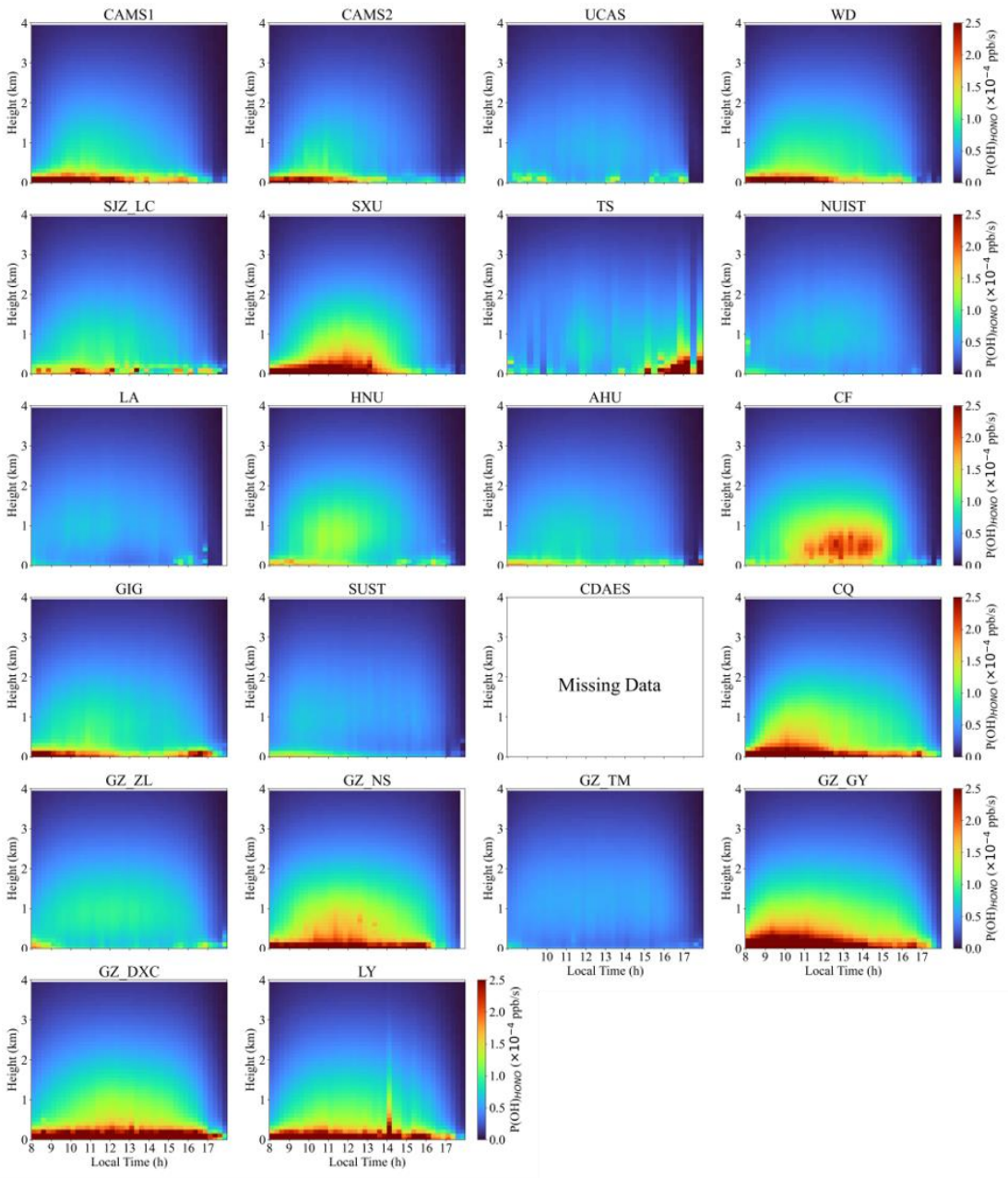

Figure S23. Autumn-mean vertical profiles of OH production from HONO photolysis.

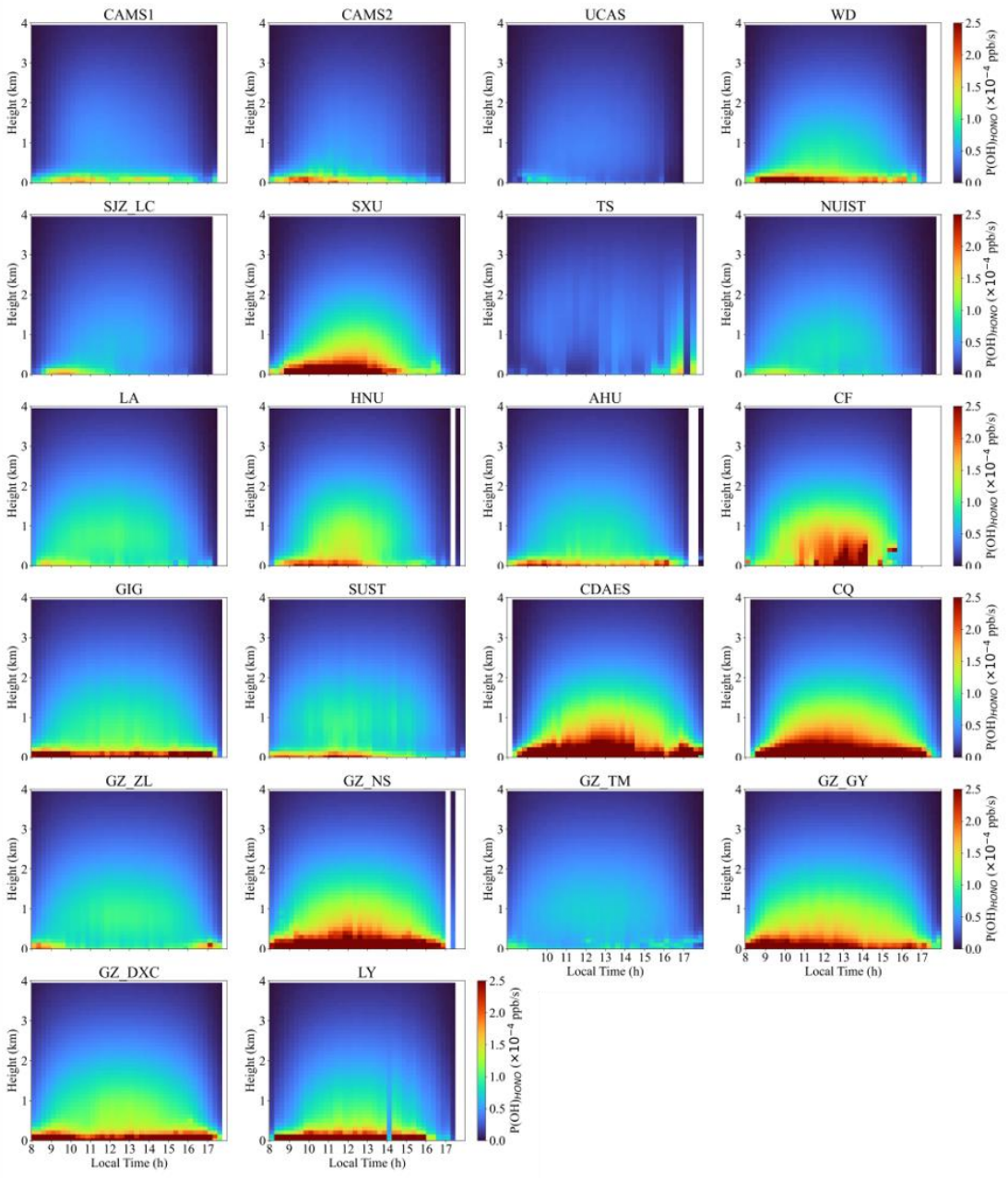

Figure S24. Winter-mean vertical profiles of OH production from HONO photolysis.

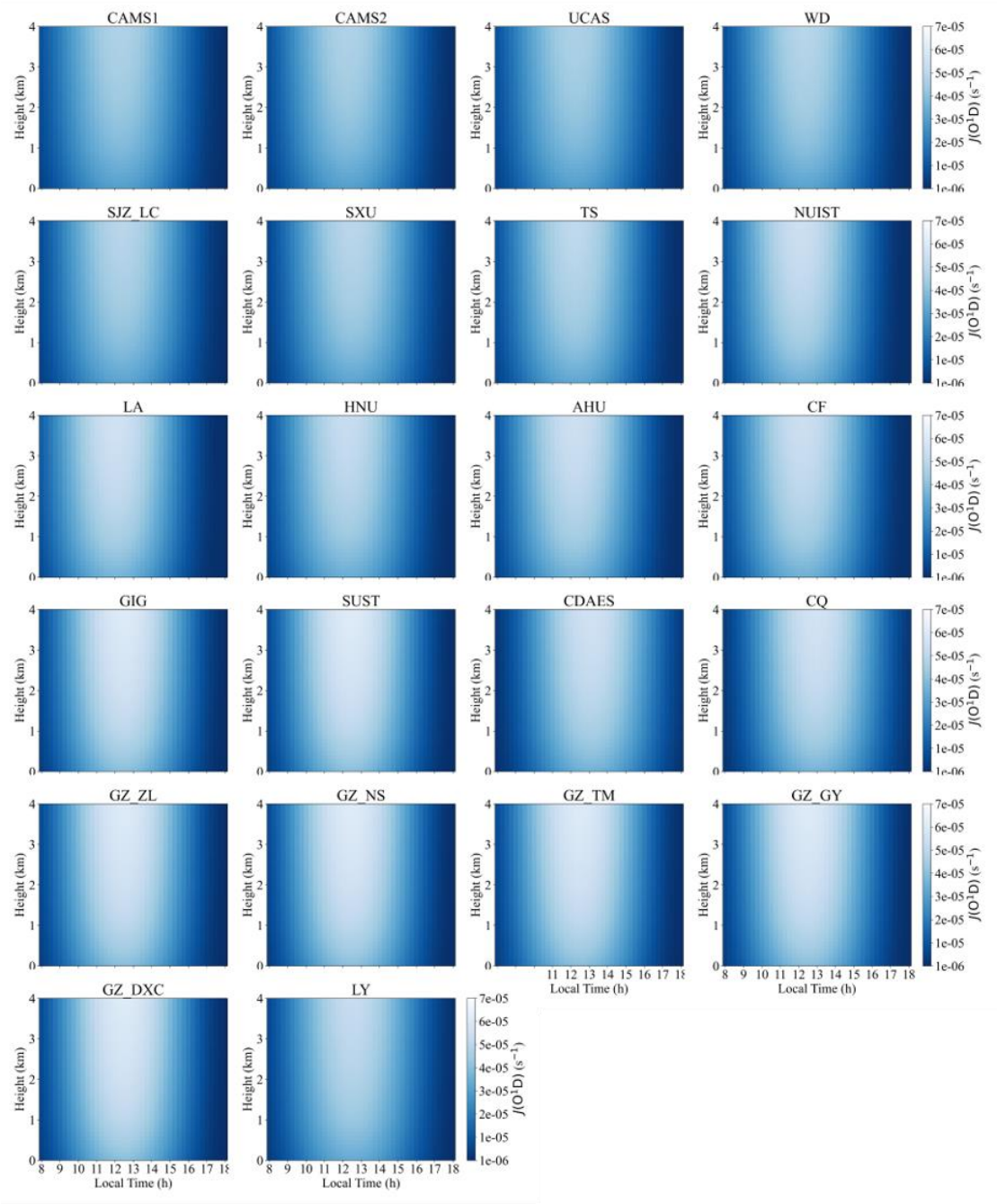

Figure S25. Spring-mean diurnal vertical profiles of the O_3 photolysis frequency, J($O(^1D)$).

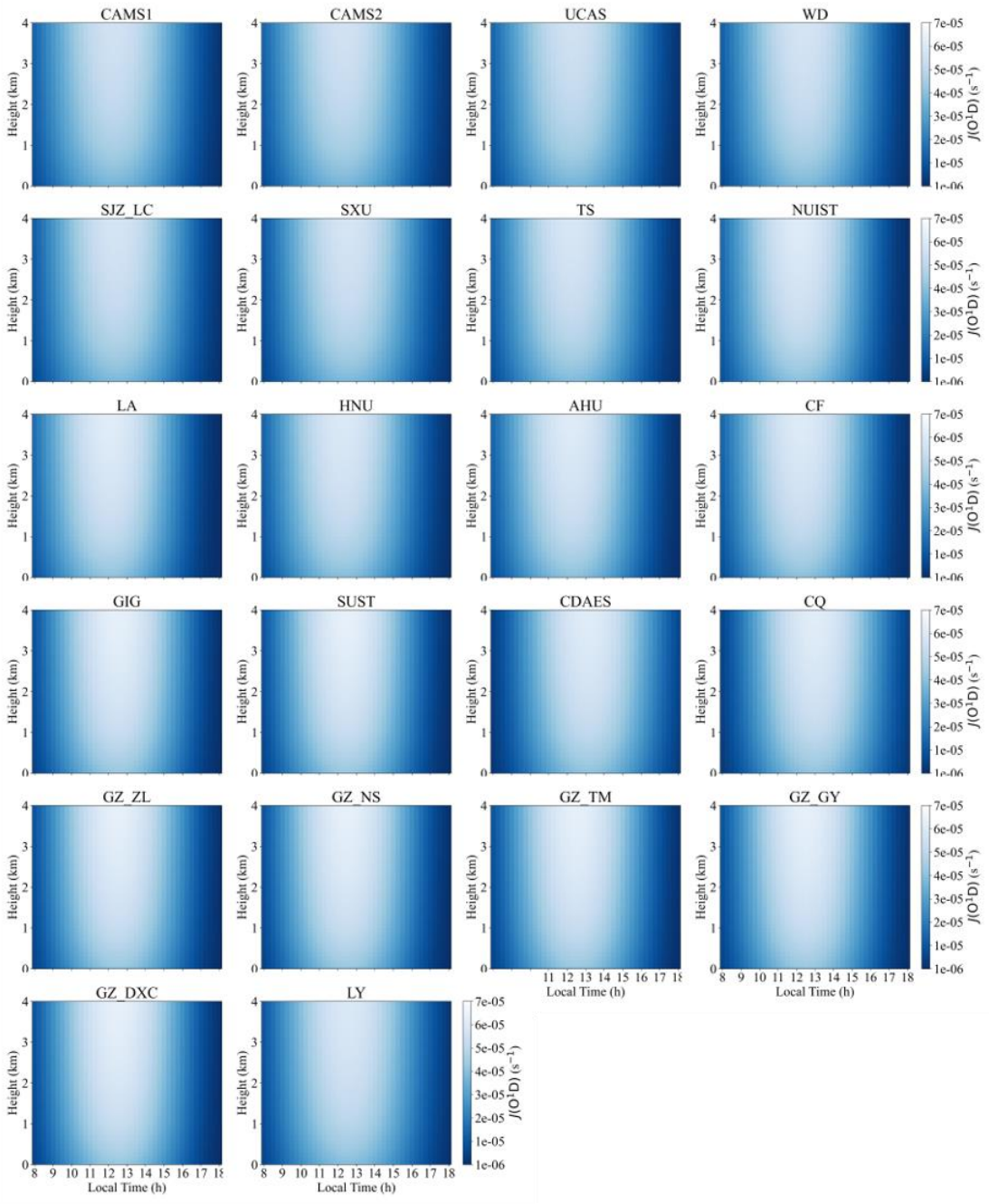

Figure S26. Summer-mean diurnal vertical profiles of the O_3 photolysis frequency, J($O(^1D)$).

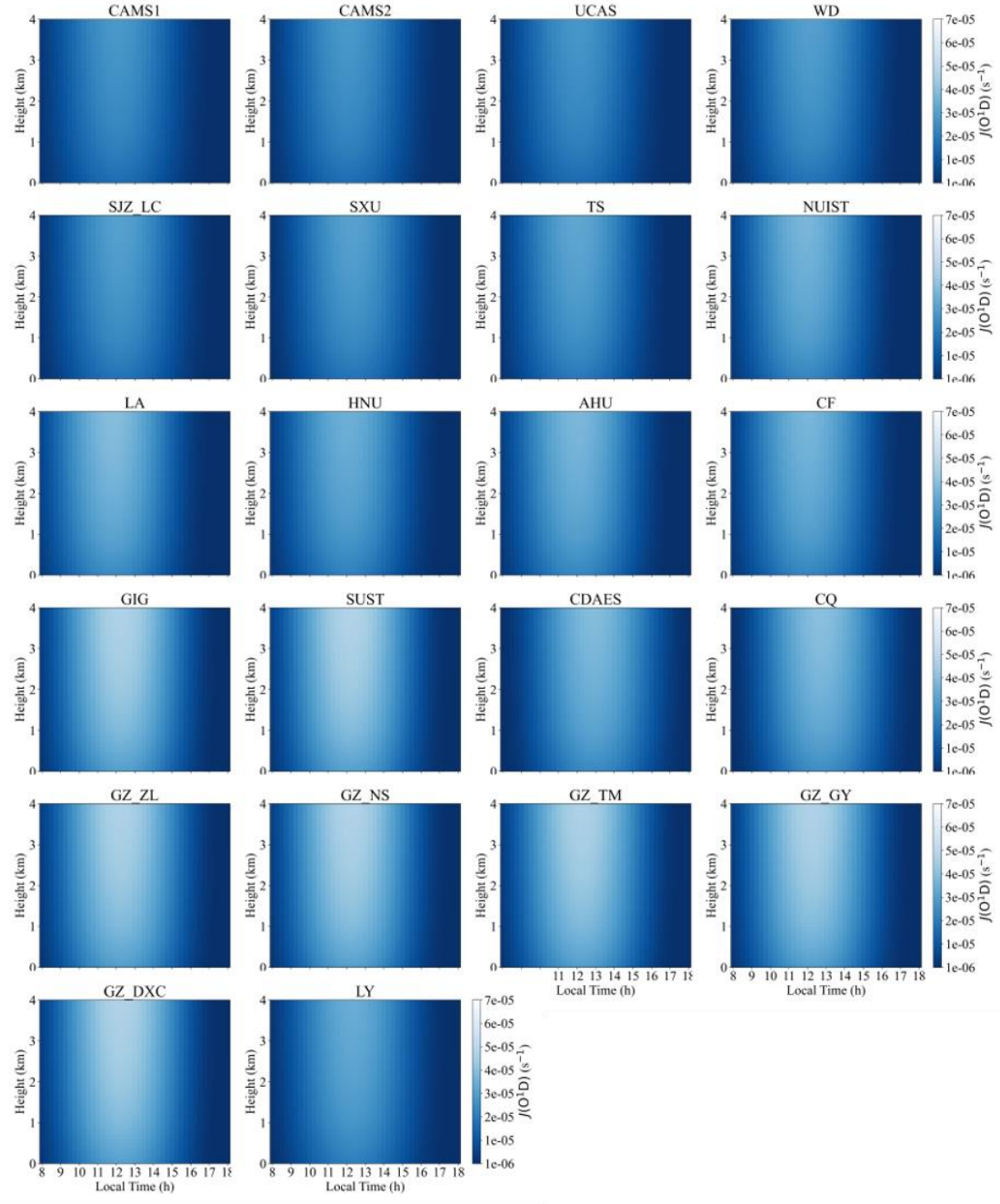

Figure S27. Autumn-mean diurnal vertical profiles of the O_3 photolysis frequency, J($O(^1D)$).

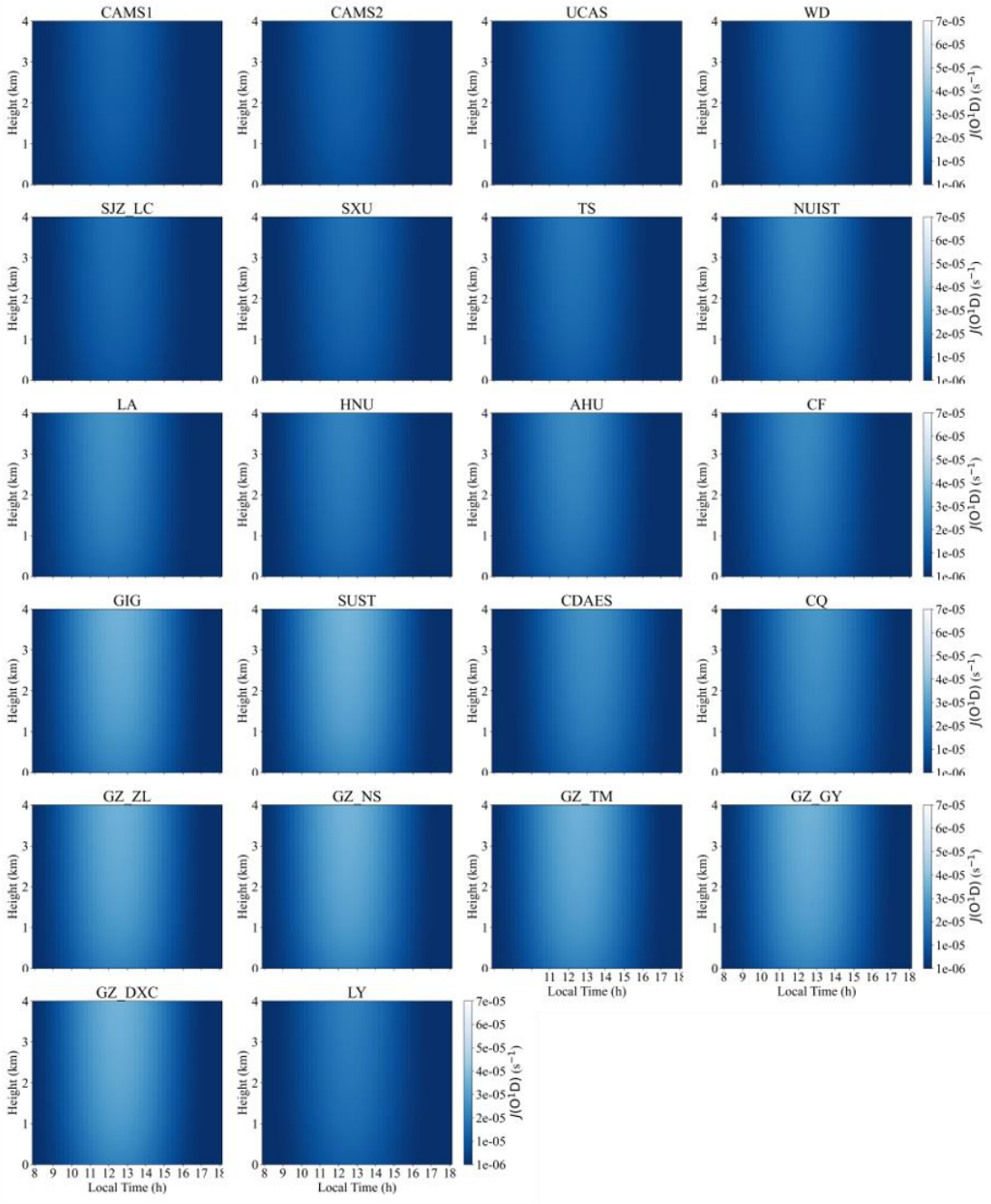

Figure S28. Winter-mean diurnal vertical profiles of the O_3 photolysis frequency, J($O(^1D)$).

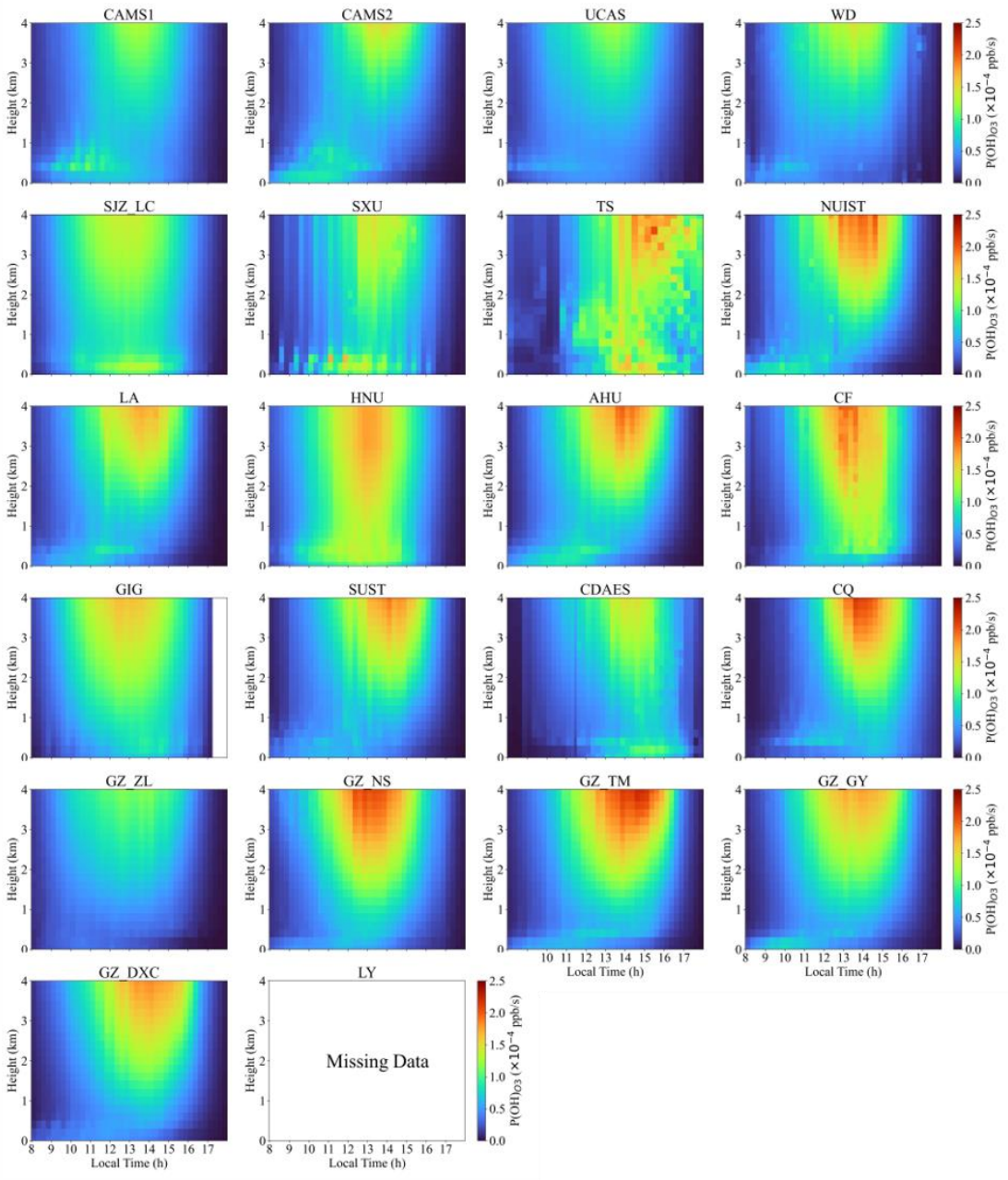

Figure S29. Spring-mean vertical profiles of OH production from O_3 photolysis.

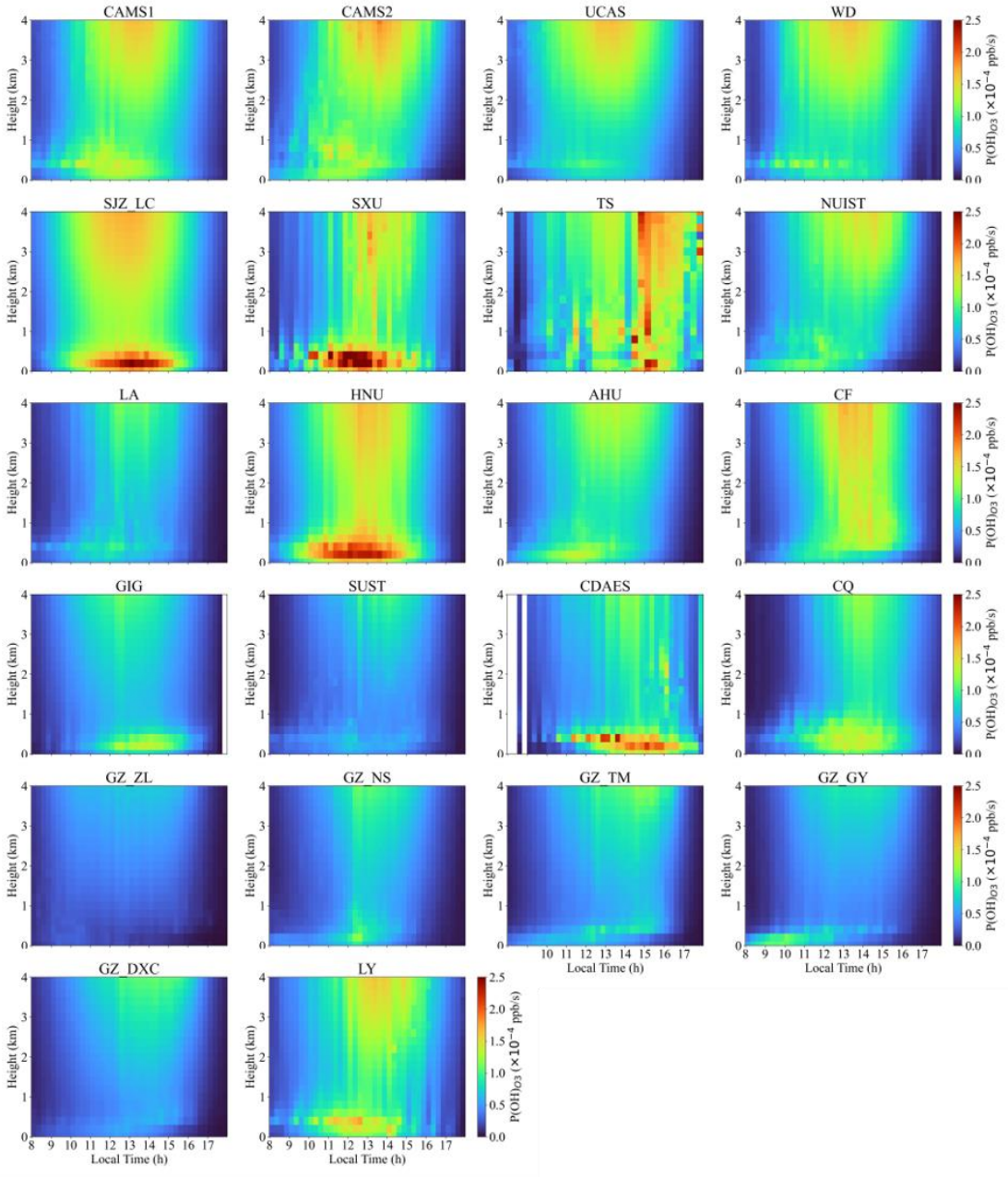

Figure S30. Summer-mean vertical profiles of OH production from O_3 photolysis.

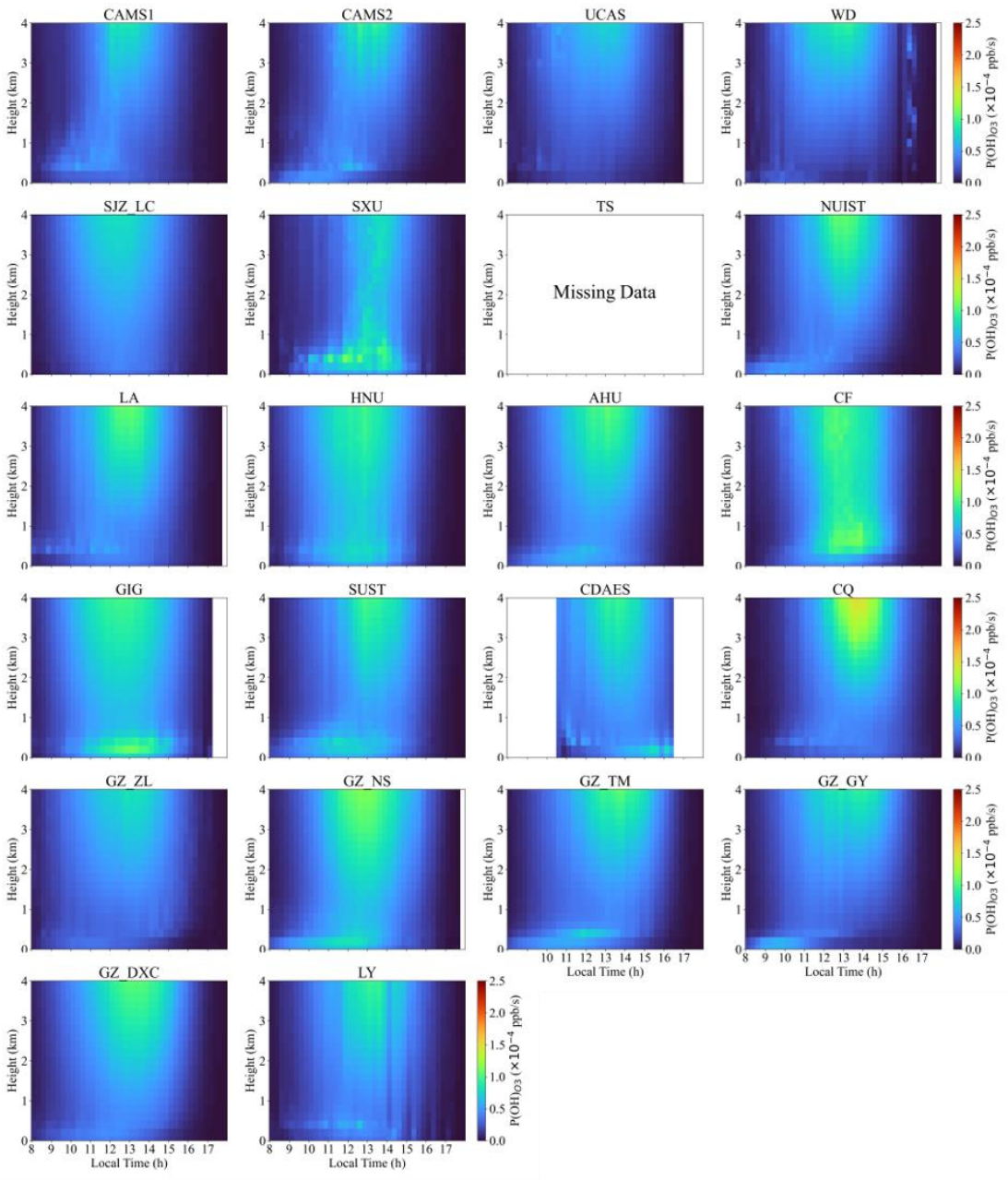

Figure S31. Autumn-mean vertical profiles of OH production from O_3 photolysis.

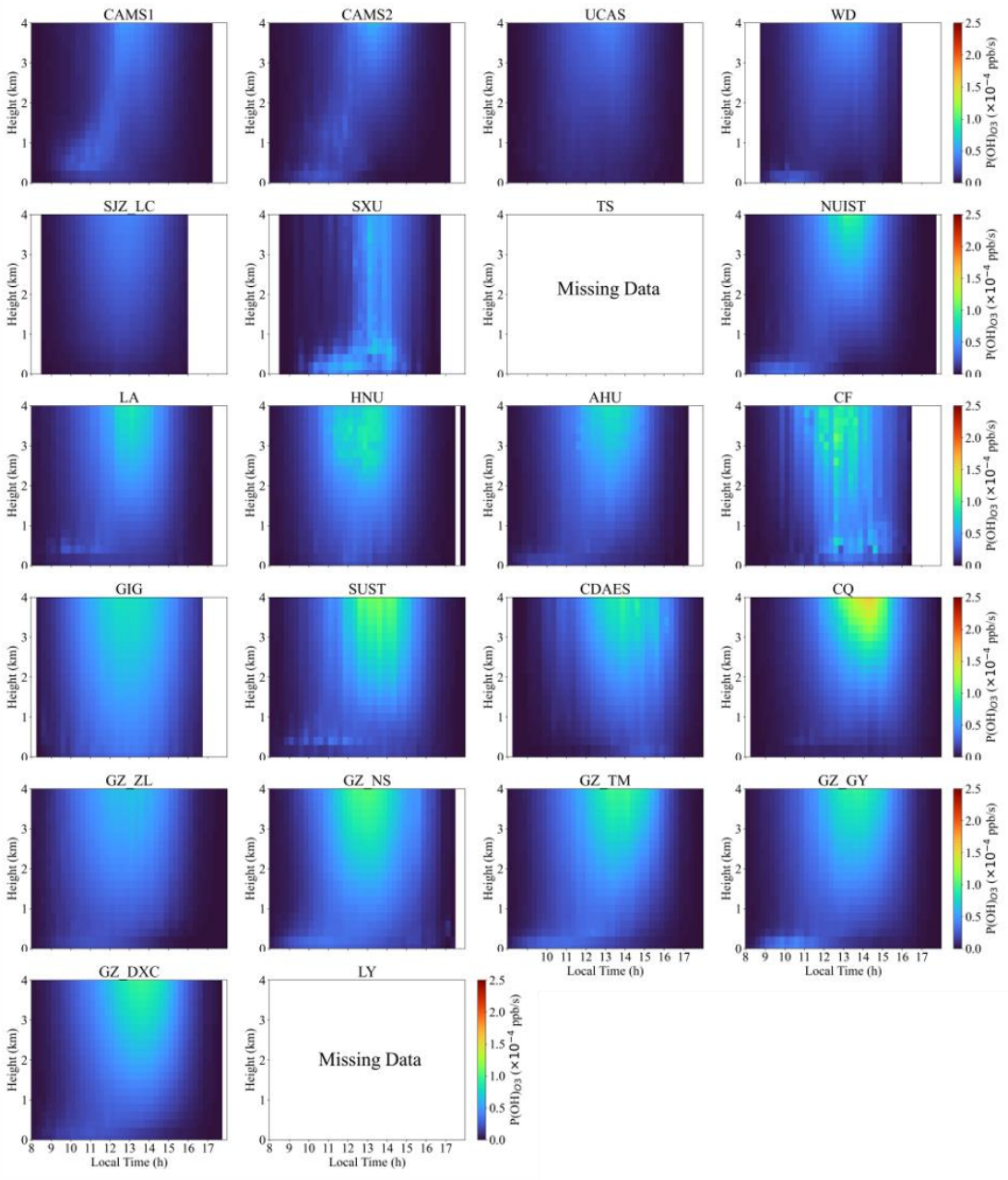

Figure S32. Winter-mean vertical profiles of OH production from O_3 photolysis.